ABSTRACT

Title of Thesis: USING ECOSYSTEM NETWORK ANALYSIS TO QUANTIFY FLUID FLOW

Michael J. Zickel, Master of Science, 2005

Thesis directed by: Professor Robert E. Ulanowicz
University of Maryland Center for Environmental Science
Chesapeake Biological Laboratory

A type of network analysis successfully demonstrated to quantify growth and development in ecosystems is applied to the purely physical phenomenon of fluid flow. Simple two-dimensional models of fluid flow are created and represented as networks of nodes and transfers or flows between nodes. Modeling flow data as a network enables the calculation of indicators or indices that quantify the activity and organization of the represented flow field. The method of cellular automata is used to create three flow field examples, two of which introduce obstacles in the flow field to disrupt the otherwise uniform flow. Four well understood examples from fluid dynamics are described analytically and then analyzed as networks. These conceptual examples of fluid flow demonstrate the utility of network analysis as a method of quantitatively characterizing complex patterns of fluid flow.

USING ECOSYSTEM NETWORK ANALYSIS TO QUANTIFY FLUID FLOW

by

Michael J. Zickel

Thesis submitted to the Faculty of the Graduate School of the
University of Maryland, College Park, in partial fulfillment
of the requirements for the degree of
Master of Science
2005

Advisory Committee:

Professor Robert E. Ulanowicz, Chair
Professor William C. Boicourt
Dr. Ming Li

Dedication

To Susan, without whom this would not have been possible.

Acknowledgements

First and foremost, I would like to acknowledge my advisor, Bob Ulanowicz, for his unwavering enthusiasm and support throughout my four years at CBL. He always made himself available whenever I was in need of advice, and I always came away from our discussions with rekindled inspiration and focus. His knowledge and guidance extended far beyond the lab and science, and I learned more from Bob than I am able to fully articulate. I will always recall our exhilarating flights over Chesapeake Bay and the first time Bob exclaimed to me, "You've got the CON."

I am very grateful to Stefano Allesina who provided me with C code for calculating several of the network indices used in this research and who spent many late hours tutoring me in programming. My committee members, Bill Boicourt and Ming Li, provided me with valuable insights into both the experimental and theoretical sides of physical oceanography. Walter Boynton readily shared his vast experiences as a field ecologist, balancing my "flute music" with the solid, deeper tones of reality. Jon Anderson reviewed portions of my computer program and made useful suggestions for improving the calculations. Karen Berquist and Michael Webber were kind enough to read over the entire manuscript and provide helpful editorial comments. Sarah Greene, Kim Makita, George Waldbusser, Mike Rearick, and many other fellow students at CBL engaged in thoughtful discussions on a variety of topics in environmental science that I found both inspiring and humbling.

Gina Coelho and Ecosystem Management & Associates, Inc. were generously flexible in allowing me to pursue my degree while providing me the opportunity to gain experience as an environmental scientist and consultant.

Finally, I gratefully acknowledge the daily sacrifices made by my family, Katherine, Peter, and my wife Susan, who gave me the precious and irreplaceable gift of time.

Table of Contents

List of Tables

List of Figures

Chapter 1: Introduction to network analysis and its application to fluid flow

Networks are used to represent natural systems in such a way that the system of interest is described both quantitatively and holistically. One of the challenges of applying quantitative methods of analysis to natural systems is defining the extent of the system (i.e. its boundaries) as well as its internal activity (i.e. exchanges of energy) in a manner that crucial exchanges, either external or internal, are not left out. This challenge is amplified as systems increase in size and complexity. Another challenge ensuing from the quantitative analysis of large-scale, complex systems is determining how to best interpret the data. With high-speed computer processing readily available even in most personal computers, generating copious amounts of data describing a natural system has become almost commonplace. Devising quantitative methods to analyze that data and holistically characterize a system in well-defined terms is less common. Examples of complex systems can be found in any number of disciplines, including thermodynamics, meteorology, oceanography, economics, social systems, and ecology. The focus of this research is on fluid flow, particularly as it pertains to problems in oceanography, and the network analysis approach used here parallels the successful application of the same analysis to ecosystems in ecology, so the remainder of the discussion will be limited primarily to those two fields. It is worth noting, however, that this approach to describing complex systems is readily applicable to the other disciplines mentioned above. Because network analysis has been well established in ecosystem ecology, initial discussion will concern that field; however, the main purpose of this research is to analyze fluid flow. Following the derivation of the network indices used to characterize systems, several

basic, well-understood examples of fluid flow will be analyzed to demonstrate the potential contribution of network analysis to the study of complex flow fields.

In ecosystem ecology, large-scale models are used to assess the state of an array of organisms interacting with each other and their environment, often with the intent of first establishing and subsequently monitoring the health or development of the ecosystem. This type of ecosystem model pioneered quantitative, system-level analyses in ecology (Lindeman 1942, Odum 1969), and ultimately lead to the network approach described here.

A network can be defined as a collection of elements, usually referred to as nodes or compartments, where individual elements are joined together by a type of interaction or communication, often called a connection or a transfer. For example, in a two-compartment network describing a predator-prey relationship, one compartment would represent the predator the other compartment would represent the prey, and the interaction would be the trophic transfer of energy from prey to predator. An advantage of network analysis is that networks are easily depicted in diagrams, which can often reveal characteristics of a system that may not be as obvious when viewing the data in other formats (Figure 1-1 predator-prey interaction with table of data).

Network analysis places greater emphasis on the transfers between nodes rather than the characteristics of individual nodes (Ulanowicz 1986a). Focusing the analysis on the transfers generates results that describe the dynamics of the system as a whole.

1.1 Rarity and the beginnings of network theory

Network analysis as it is discussed here is grounded in the field of information theory, which in turn derives its foundations from probability theory (Tribus and McIrvine 1971). In probability theory the rarity of an event, A, is quantified as

$$S(A) = -k \log p(A) \tag{1.1}$$

where p(A) is the probability of event A occurring, k is a scalar constant, and S(A) is the rarity of event A. Relating the rarity or indeterminacy of an event within a system to the logarithm of the probability of the event was first accomplished by Ludwig von Boltzmann in 1872. If one does not expect event A to happen often, then p(A) is by definition small and S(A) becomes large, meaning that event A rarely occurs. A system continuously in a state of flux, such as an ecosystem, might best be described by defining the events that connect its constituent components. Therefore, it becomes desirable to understand how one event affects the indeterminacy of any subsequent events. Given the occurrence of event B, the probability of event A becomes p(A|B) (i.e. the conditional probability of A given B), and the indeterminacy of event A decreases to

$$S(A \mid B) = -k \log p(A \mid B) \tag{1.2}$$

The reduction in the indeterminacy, S(A) – S(A|B), is also a measure of the constraint that the occurrence of event B places on event A, and may be written as,

$$S(A) - S(A \mid B) = k \log\left(\frac{p(A \mid B)}{p(A)} \right) \qquad 1.3$$

In anticipation of generalizing the analysis to include more than two events, one may employ Bayes' Theorem (Joyce 2003) to define p(A,B) as the joint probability that events A and B occur in combination, and equate p(A|B) with the quotient p(A,B)/p(B), so that (1.3) becomes,

$$S(A) - S(A,B) = k \log\left(\frac{p(A,B)}{p(A)\,p(B)} \right) \qquad 1.4$$

Since events A and B represent any two arbitrary events occurring within the scope of a larger system comprised of many events, one can calculate the average mutual constraint that all system events exert on each other by multiplying (1.4) by the joint probability associated with each pair of events (i.e. $p(A_i,B_j)$) and summing over all event pair combinations, as denoted by the indices *i* and *j*.

$$\sum_{i,j} p(A_i,B_j)\left[S(A_i) - S(A_i,B_j)\right] = k \sum_{i,j} p(A_i,B_j) \log\left(\frac{p(A_i,B_j)}{p(A_i)\,p(B_j)} \right) \qquad 1.5$$

At this point the quantities to be evaluated are probabilities. To use (1.5) for evaluating systems, one must somehow relate these probabilities to measurable quantities.

1.2 Network indices as metrics of system complexity

Let the quantity T_{ij} be defined as the amount of medium transferred from compartment *i* to compartment *j* in a network. To quantify all transfers for a given network one simply sums over all *i* and *j*,

$$T_{\cdot\cdot} = \sum_{i,j} T_{ij} \qquad 1.6$$

resulting in a quantity called the total system throughput, which, as the sum of all transfers occurring within a network, is an indicator of system activity. A simplified notation is introduced in (1.6), which will be used hereafter. A dot used as the subscript indicates summation over the index it replaces. For example, $T_{\cdot j} = \Sigma_i T_{ij}$, signifies that summation occurs only over the first index, *i*. From (1.6) it should be clear that the activity of a system increases as more transfers occur or more medium per transfer is exchanged. Referring back to (1.5), the probability that subsequent transfers begin with event A_i (i.e. $p(A_i)$) is estimated as the quotient $T_{i\cdot}/T_{\cdot\cdot}$, and is the fraction of all transfers originating from compartment i. Similarly, $p(B_j) \sim T_{\cdot j}/T_{\cdot\cdot}$, and the joint probability for each pair, $p(A_i,B_j)$, is estimated as $T_{ij}/T_{\cdot\cdot}$. Substituting these measurable transfers into (1.5) yields

$$AMC = k\sum_{i,j}\frac{T_{ij}}{T_{..}}\log\left(\frac{T_{ij}T_{..}}{T_{i.}T_{.j}}\right) \qquad 1.7$$

where AMC is the abbreviation for "average mutual constraint." In the field of information theory the terms "constraint" and "information" are used synonymously, and from this point forward the quantity in (1.7) will be referred to as the average mutual information, or AMI. A more thorough derivation of the AMI is found in Ulanowicz (1986a, 2000), and a complete background on the origins of network analysis in information theory is found in Rutledge et al. (1976).

Although quantitative and based on measured units of transfer, the AMI is also scaled by the as yet undefined scalar, k, which somewhat limits its utility. By equating k to the total system throughput, T.., the AMI takes on physical dimensions and becomes an indicator of both the organization inherent in a system and the system activity. This new quantity is called the system ascendency (Ulanowicz and Mann 1981),

$$A = \sum_{i,j} T_{ij}\log\left(\frac{T_{..}T_{ij}}{T_{.j}T_{i.}}\right) \qquad 1.8$$

and is applied in ecology as a means of quantifying growth and development in ecosystems (Ulanowicz 1986a). The ascendency, like the AMI, is an indicator of system organization, but it is also dependent on system activity. Given two systems with the same AMI, the system with the greater T.. will have a greater A. Intuitively, this should make sense; given two systems that transfer energy with the same level of coherent

organization, the system transferring more energy should be considered more developed. The ascendency index quantifies that distinction.

Additional network indices that define limits on the A and provide for losses to the environment that inevitably occur with physical-biological systems are discussed elsewhere (Hirata and Ulanowicz 1984, Ulanowicz 1986a, Ulanowicz 1986b).

Ascendency Theory is related to the principle of Maximum Entropy Production (MEP), which has its foundations in thermodynamics, in that both approaches seek to quantify system level dynamics based upon the activity of system components. MEP maintains that the non-equilibrium steady state is the one in which entropy is produced at the maximum rate, subject to the physical constraints defining the system (Kleidon and Lorenz 2005; Dewar 2005). Characterizing systems according to their entropy corresponds to measuring their disorganization; whereas A is a measure of system organization. Hence the two methods of characterizing systems are complimentary. Furthermore, Ascendency Theory has the capability of assessing the organization at the level of microscale transfers (or flows), and changes at this level should result in different rates of MEP at the macroscale system level (Ulanowicz and Zickel 2005).

Because the A as it is written in (1.8) is homogeneous with respect to the individual transfers, T_{ij}, one can immediately write the sensitivities of the A to any arbitrary transfer, T_{pq}, as

$$\frac{\partial A}{\partial T_{pq}} = \log\left(\frac{T_{pq}T_{..}}{T_{.q}T_{p.}}\right) \qquad 1.9$$

The transfers to which the ascendency is most sensitive are those that are limiting in the sense of nutrient availability in an ecosystem, or are indicative of bottlenecks in a fluid flow field (Ulanowicz and Baird 1999).

1.2.1 A simple example: intuitive and calculated organization in a four-compartment network

A network consisting of four nodes and no communication (or transfers) with the outside environment (Figure 1-1) is a very unrealistic representation of a natural system. However, assessing organization in such a network can be done by inspection, and the corresponding value for the network ascendency can be easily calculated by hand. Such a demonstrable example can be useful for understanding this approach before it is applied to more complex and less intuitive systems (Ulanowicz 1986b).

Equal amounts of a medium (e.g. carbon, energy, a fluid, etc.) are transferred between four compartments labeled A, B, C, and D (Figure 1-1). For simplicity, the magnitudes of all transfers within each network are made equal, and the total amount transferred (i.e. T..) is held constant across all three networks. A qualitative assessment of the organization in the three networks should lead one to determine that the network in Figure 1a transfers the same amount of medium in a much less organized fashion than the network depicted in Figure 1c.

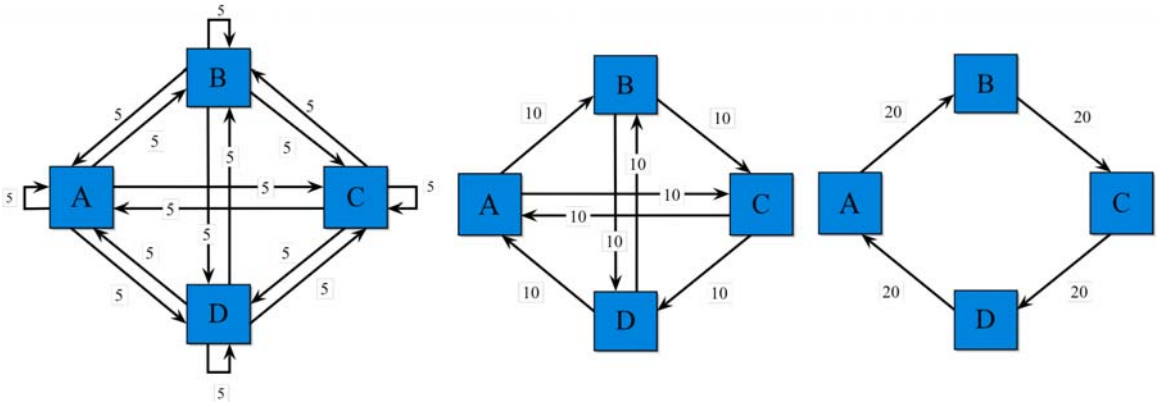

a b c

Figure 1-1. Three stages in the evolution of a four compartment network with the overall network activity held constant: a) minimally organized, b) more organized, and c) maximally organized. Numbers represent the magnitude of the transfer and arrows indicate the direction of the transfer.

If one thinks in terms of an ecosystem where each compartment represents an organism and transfers between organisms represent predation, then clearly the least organized state possible is the one in which every organism eats every other organism, including itself (Figure 1a). The transfer of energy in such an ecosystem would seem haphazard and chaotic, and would possess no discernable direction of development. The representative network would demonstrate no preferred pathways, nor would it reveal any permanent hierarchy or structure in the system.

If the maximally connected network is also the least organized network, then it stands to reason that reducing the number of connections should increase the inherent organization of the network. In an intermediate network (Figure 1b), half of the transfers are eliminated leaving two transfers per compartment, and the amount of medium

transferred is doubled (to 10 units) to maintain the same TST. Organization in the network increases as half of the transfers are now unidirectional. Extending the argument, one would conclude that the most highly organized state possible in a four compartment network is the one in which each compartment transfers medium to only one other compartment, or in terms of an ecosystem, each organism preys upon only one other organism (Figure 1c).

This qualitative assessment of organization in a four-compartment network is based solely upon the magnitudes (which in the example above are all equal, but this need not be the case) and directions of the transfers occurring between the nodes in the network. A quantitative assessment is dependent upon those same network attributes.

Quantifying organization in each of the three four-compartment networks in Figure 1 is accomplished by calculating the network indices T.., AMI, and A as shown in equations (6) through (8). Throughout this thesis, $\log_2$ is used in the calculations making "bits" the unit of transfer. The results of the calculations, which can easily be performed by hand, for the three networks (Figure 1) corroborate the initial, qualitative assessment of organization in a four-compartment network (Table 1). The minimally organized and maximally connected network (Figure 1a) has an AMI equal to zero bits, and therefore, an A equal to zero flow bits.

Table 1. Network indices describing the three four-compartment networks in Figure 1-1 where a) is the maximally connected minimally organized network, b) is the intermediate network, and c) is the minimally connected maximally organized network.

Index	Minimally Organized Network (a)	Intermediate Network (b)	Maximally Organized Network (c)
$\mathbf{T_{ij}}$	5	10	20
T..	80	80	80
AMI	0	k	2k
A	0	80	160

When the number of transfers per compartment is reduced to four (Figure 1b) the result is a more organized system with the AMI equal to k bits and the A equal to 80 flow bits. Further reducing the number of transfers per compartment to two—the minimum number for a viable network—results in the maximally organized case, where the AMI = 2k bits and the A = 160 flow bits. It is hypothesized that, in the absence of perturbations, systems will develop towards ever increasing values of the A (Ulanowicz 1986a, Ulanowicz 1997). Because perturbations are prevalent at all levels in natural systems, it is unlikely that any natural system (e.g. an ecosystem) will achieve maximum organization. The important role that perturbations (e.g. a hurricane or major outbreak of disease) play in the development of natural systems is emphasized by noting that the maximally organized network (Figure 1c) is also the network most susceptible to disruption, because, if one of the transfers is interrupted, the system is no longer fully connected.

This oversimplified example can easily be adjusted to better represent a natural system by including an external input and output, and showing preferred transfers that

dominate over weaker ones rather than altogether eliminating transfers between nodes as was done above. Increasing only slightly the complexity of a simple four-compartment system quickly places any qualitative assessment of organization on somewhat shakier ground. A hybrid four-compartment network (Figure 1-2) representing a somewhat more realistic four-compartment system has T.. equal to 191, AMI equal to 1.15k bits, and A equal to 219 flow bits.

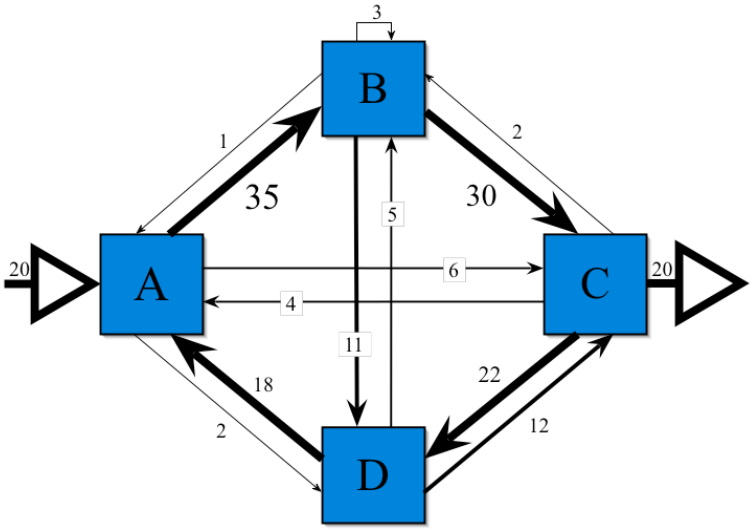

Figure 1-2. A four-compartment network displaying dominant internal transfers as well as transfers with the external environment. The magnitude of each transfer in flow units is indicated by the number on each arrow, and the arrows indicate the direction of transfer.

It is probably not intuitively obvious that the transfers in this network are any more or less organized than the similarly structured intermediate network (Figure 1-1b). However, comparing the AMI of the two networks indicates that the organization of information in the hybrid network, where the AMI = 1.15k bits, is greater than the organization of information in the intermediate network, where the AMI = 1k bits, despite the fact that the latter has fewer transfers. The network ascendency for the hybrid

network (Figure 1-2) is much greater than even the maximally organized network (Figure 1-1c), because more medium is transferred through the network making T.., which scales the A, greater. If the transfers are reduced proportionately so that the T.. = 80, the AMI will still equal 1.15k bits, and the A will be reduced proportionately to equal 92 flow bits.

The purpose of these two examples is to demonstrate how network indices reflect organization in systems. For a more thorough discussion on this subject refer to Ulanowicz (1986a, 1986b, 1997).

1.2.2 Network analysis applied to ecosystems

The simplified example provided above illustrates the basics of a network analysis approach to quantifying complex systems. A principal goal of this thesis is to demonstrate that the same approach is applicable to the study of complex systems of fluid flow. To help support that argument, a brief discussion on the evolution of network analysis as a method for quantifying ecosystems is presented.

Ecology can be defined as the study of the interactions between living organisms and their physical environment. Such a scope has traditionally required ecologists to consider relatively large spatial regions (i.e. on the order of acres) over time periods ranging from seasons to decades. Early research in ecology focused on the study of individual biological communities, and was dominated by the collection of experimental data, rather than theoretical concepts. It was not until Lindeman (1942) published his

landmark paper describing trophic exchange in ecological communities that the modern concept of the ecosystem was introduced (Hagen 1992), and it has served as the fundamental element in ecology ever since. Defining and then describing a system of diverse components whose very interactions are the primary, if not only, reason for linking them together in terms that are both quantitative and meaningful to other scientists has been a perpetual challenge since the advent of ecosystem ecology (Hagen 1992). Early attempts to describe ecosystems in quantitative terms resulted in the generation of large quantities of data and required creative means of summarizing and displaying the results (Odum 1957, Hagen 1992). Complex diagrams comprised of multiple symbols connected by weighted lines, where each visual nuance conveyed some quantitative meaning, were devised to accomplish this difficult task. An experienced eye was required in order to fully comprehend the diagrams (at times referred to as "spaghetti diagrams" by the trained and untrained alike) in their entirety, and to understand the processes comprising the ecosystem (Boynton personal communication). Quantitative methods attempting to establish the ecosystem based on the connections between organisms were evolving, but universal definitions applicable to all varieties of ecosystems were lacking. In his seminal paper describing ecosystem succession, Eugene Odum (1969) defines quantitative benchmarks delineating stages of ecosystem development. For the first time, ecosystem ecology had a set of metrics by which the maturity and relative health of individual ecosystems could be judged. For many ecosystem scientists, Odum's twenty-four criteria issued an implied challenge: to develop a quantitative method to analyze the diversity of ecosystem data in such a way that the results can be directly compared to Odum's criteria. One such method—the

method described in this thesis—expands on the "spaghetti diagrams" framework by adapting formulas from the field of information theory to quantify ecosystem characteristics. As noted above, this is done by representing a group of organisms and their collective exchanges as a network, and then applying the mathematical formulas to characterize networks by the amount of medium they transfer, and how random or organized those transfers appear.

Since this thesis takes only the initial step in analyzing complex patterns of fluid flow, an example of a system of comparable complexity is taken from ecosystem ecology to demonstrate that network analysis is capable of evaluating large, complex, natural systems. This example, coupled with the more fundamental examples from fluid dynamics described in Chapter 3 of this thesis lays the groundwork for applying network analysis to current problems in interpreting complex fluid flow patterns, such as those encountered in modeling instabilities, eddies, and turbulent flow.

The mesohaline ecosystem of Chesapeake Bay has been represented as a network of 36 nodes with exchanges of carbon as the medium of transfer between the nodes and the surrounding environment (Figure 1-3; Baird and Ulanowicz 1989). In this network, transfers of various forms of carbon occur between organisms across trophic levels, and between organisms and the physical environment. Large quantities of data including standing stocks associated with each compartment, rates of carbon intake, respiration, production, and egestion for each compartment, and rates of transfer between linked nodes are required to describe this ecosystem. The network is analyzed to reveal the

dependence of a particular species on the abundance or presence of another species, the dependence of a trophic group on a single transfer or set of transfers, and to investigate the overall dependency of the ecosystem on seasonal cycling. Several previously unrecognized characteristics of the Chesapeake Bay ecosystem were revealed, not through the acquisition of additional experimental data, but by integrating available data into one quantifiable analysis.

Subsequent analysis on the Chesapeake Bay ecosystem (Ulanowicz and Baird 1999) quantifies seasonal cycling of nutrient limitation within the ecosystem. The network approach correlates well with the traditional analysis of nutrient limitation introduced by Liebig, but also reveals nutrient controls that would not otherwise have been observed had the ecosystem been represented as a collection of individual populations rather than as a network of transfers.

1.3 Application to the study of fluid flow

A network analysis approach, demonstrated to be successful in ecology, is now applied to the quantification of fluid flow fields, which can be represented as networks of nodes and flows between nodes. A change in nomenclature is adopted to distinguish between the different constraints that exist when representing a fluid flow field as a network rather than an ecosystem. A single flow from grid point *i* to grid point *j* will be represented as f_{ij} instead of the familiar T_{ij} from this point forward. Unlike transfers within an ecosystem, which may occur between any two nodes regardless of their spatial

juxtaposition, flows in a flow field are limited to adjacent nodes. In a two-dimensional flow field, flow from any compartment must occur only between one (or more) of the neighboring nodes. A thorough theoretical expansion of this type of network analysis to the investigation of fluid flow has recently been outlined (Ulanowicz and Zickel 2005).

1.3.1 The problem of interpreting output from large scale simulation models

Examples of complex patterns of fluid flow resulting from simulation models are analogous in many ways to other large-scale complex systems (e.g. ecosystems, socio-economic systems, etc.). In each case, some quantity of a chosen medium (e.g. fluid, carbon, currency, etc.) is transferred from one point to another at a particular rate of exchange. If both the amounts and transfer rates are known or measurable, then a network representing the system can be created and analyzed to characterize the transfers of the system as ordered or stochastic. In large eddy simulation models flows are separated or filtered by their spatial scale, so that large-scale flows can be simulated explicitly while the influence of small-scale flows is simulated through an averaging technique. Large scale turbulent flows are energy producing and it is assumed that the unresolved small-scale (i.e. subfilter or subgrid) flows dissipate the energy into heat lost to the surrounding environment (Mason 1994). Quantifying the large-scale flows and representing the flows as a network would allow the organization of the flow field to be characterized in terms of its ascendency. As the flow field becomes more turbulent the number of large-scale flows should decrease as more of the flows become subgrid flows, and the ascendency index should decrease proportionately. With enough

experimentation, the ascendency index may be able to serve as a guide in determining the minimal scale at which large-scale flows are explicitly calculated. A minimum acceptable value of A, representing the minimum acceptable level of stochasticity in the large-scale flows, would allow for a comparison of different attempts at simulating the same turbulent flow field using an index, A, that is independent of the model.

In a process analogous to the steps taken by ecologists who first developed methods for quantifying ecosystems, oceanographers and meteorologists achieving results from simulations of complex fluid flow are exploring methods of holistically interpreting their results (Li personal communication). Network analysis, as demonstrated in this thesis, has the potential for providing an equally satisfactory tool for oceanographers and meteorologists as it has proven to be for ecologists.

Chapter 2: Cellular automata as a method of generating simple flow fields for analysis as networks

To this point, data relevant only to the field of ecosystem ecology has been presented in support of a network analysis approach to investigating fluid flow. The purpose of this chapter is to describe three simple flow field models created to generate data more representative of fluid flow. Each model is created by employing the method of cellular automata (CA) to simulate the motions of a fluid in three flow fields. The CA method is used for three main reasons: 1) it is simple to create a reasonable simulation of fluid motion and to incorporate obstacles within the flow field; 2) the groundwork for this approach (Ulanowicz 2000) utilized CA in modeling the migration of animals across landscapes; and 3) the data produced with CA are readily suitable for network analysis. A good introduction to the CA technique and its application to simulating physical systems, including fluid flow, is found in Chopard and Droz (1998). Even though it is not the intent of this paper to provide an accurate simulation of the motions of an actual fluid, CA have been used for that very purpose. Two-dimensional wave propagation models and boundary layer models have been simulated using CA (Chapard and Droz 1998), and ocean circulation patterns have been modeled and analyzed for both two-dimensional (Salmon 1999a) and three-dimensional flow fields (Salmon 1999b) using a Lattice-Boltzmann technique very similar to the CA method.

2.1 Flows across a two-dimensional flow field

A simple two-dimensional flow field is created as a square grid of 20 x 20 cells, where each cell is identified by a single numerical index and all cells in the grid are numbered consecutively from 1 to 400 (Figure 2-1). "Wrap around" boundary conditions are adopted to enable continuous flow in all directions labeled: north, east, south, and west in clockwise fashion beginning at the top.

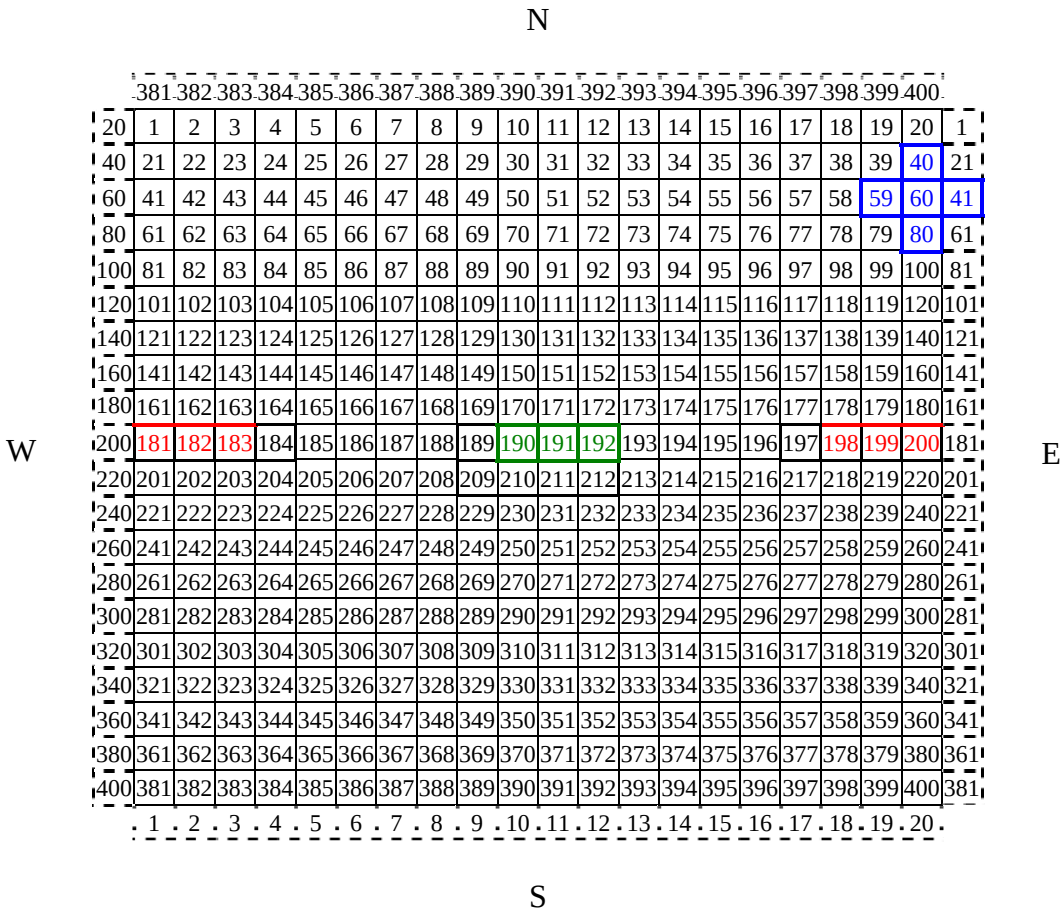

Figure 2-1. Two-dimensional flow field with "wrap around" boundary conditions. Cells highlighted in blue are discussed below. Grid points highlighted in red and green represent "barrier" cells used to create two of the flow fields referred to later in the text.

Fluid flow is simulated by the movement of particles of flow medium from one cell to a neighboring cell according to a set of simple constraints. Flow to or from any cell in the grid is limited to its nearest four neighboring cells. For example, flow occurring to (or from) cell 60 is limited to cells: 40, 41, 59, and 80 (Figure 2-2).

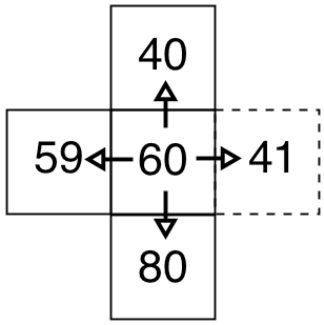

Figure 2-2. Flow from one cell (60) is limited to its nearest four neighbors.

Each cell in the 20 x 20 grid is initially allotted 100 particles with the exception of barrier cells, which contain no particles at any time during a simulation. For each time step in the simulation, every particle is required to move from its current cell into a neighboring cell, thus maintaining a constant total system throughput (f..), and ensuring a balanced network (i.e. inputs = outputs).

2.1.1 Assigning direction to flow

The direction that a particle will move varies depending on which one of five scenarios is chosen (Table 2). For example, if scenario #3 is chosen, then over the course of the simulation the particles will move South approximately 46% of the time, East and West about 25% of the time, and North only about 4% of the time. If a particle

encounters a barrier (barrier cells are present in two of the flow field examples discussed below), then it must move into one of the neighboring non-barrier cells.

Table 2. The five scenarios that set the probability that a particle will move to the North, East, South, or West of its current location. Each scenario is applied in all flow fields analyzed below.

Scenario (#)	North (%)	East (%)	South (%)	West (%)
1	25	25	25	25
2	14	25	36	25
3	4	25	46	25
4	4	20	56	20
5	2	15	68	15

Inducing movement over a flow field by assigning probabilities is an attempt to simulate both advection in a particular direction and diffusion along gradients. A greater probability of movement in one direction is akin to greater or more rapid flow in that direction with less time for, or likelihood of, diffusion in the remaining directions. A flow field without barriers and having an equal probability of flow in all four directions is akin to the maximally connected and minimally organized four compartment network described in Chapter 1, and is most representative of random, non-directional motion. Such a network, which is generated by the probabilities of scenario #1, is used as a baseline for assessing fluid flow with a dominant direction, as is produced in scenarios 2-5. Although the directional probabilities described in each scenario move particles to simulate flow in a way that is qualitatively fluid-like, the movement of the particles is not based upon the physical forces that determine the movement of an actual fluid, such as pressure gradients, continuity laws, or momentum fluxes. In either case, flows across the

flow fields represented below appear realistic, but it should be kept in mind that the directional scenarios are based entirely on probabilities.

If a fluid flowing in one direction, say to the south, were to encounter a barrier to the flow, then it is more likely that the dominant direction of the flow would be redirected perpendicular to the initial direction of the flow, that is to the east and west, rather than directly opposite. With that in mind, given that flow to the south is dominant in scenarios 2-5, it is less likely that there would be much diffusion to the north; therefore, diffusion to the east and west was permitted to exceed diffusion to the north in all scenarios with a dominant flow.

2.1.2 Network analysis applied to particles moving across a flow field

After each time step, the total number of particles transferred between each compartment in the flow field is stored in an N^2 x N^2 flow matrix, where most elements in the flow matrix equal zero. This last point is clear if one considers that flows from any single compartment are limited to its nearest four neighboring nodes, and that the flow matrix has the capacity to store flows from each compartment to every other compartment. The network indices, f.., AMI, and A are calculated from this flow matrix according to equations 1.6 through 1.8, with one alteration. The equation for the A is modified to calculate the contribution at each compartment to the overall network ascendency, and to allow each compartment's contribution towards A to be plotted over the flow field as a three-dimensional contour plot. This new quantity A_j is calculated as,

$$A_j = \sum_i f_{ij} \log\left(\frac{f_{ij} f_{..}}{M_i M_j}\right) \qquad 2.1$$

where M_i and M_j represent the total number of particles at compartment *i* and compartment *j* respectively. This modification follows the example of Ulanowicz (2000), from which the following hypothesis is adapted to address fluid flow:

> *In the absence of massive perturbations, particles representing the motions of a fluid will distribute themselves across a flow field in a way that leads to higher system ascendency.*

A massive perturbation in the context of fluid flow might be any disturbance that completely disrupts the initial pattern of flow, such that the associated network representing the flow would cease to function as a network.

2.1.3 Methods: A cellular automata program for simulating fluid flow

A program written in the C programming language was used to create each flow field, move the particles through the flow field according to the scenarios described above for a chosen number of time steps, and to calculate the network indices after each time step. All three-dimensional contour plots depicting a distribution of values over the flow field were produced using the R programming language (R Development Core Team 2003). Neither program is appended to the thesis, but both are available from the author upon request.

A flow field consisting of a grid of 1's and 0's is read into the program, and defines the size of the flow field as well as the free flow (0's) and barrier (1's) grid points in the flow field. All free flow grid points are then populated with 100 particles. At each time step, every particle must move to one of its four neighboring grid points. If a particle attempts to move to a barrier grid point it is redirected towards one of the three remaining grid points.

A particle that does not encounter a barrier always moves according to the probability assignments defined by the chosen scenario (Table 2). Once a particle encounters a barrier, though, a more deterministic assignment is applied. For example, if a particle moving towards the south encounters a barrier blocking its path, then it is redirected either towards the west or the east, depending on which half of the flow field it is located: particles on the western half move west, and particles on the eastern half move east (Figure 2-3). The same assignments apply for a particle encountering a barrier when moving north. If a particle encounters a barrier when moving east or west, then it is directed in the opposite direction. These directional assignments, although arguably simplistic for describing fluid movement, create a reasonable simulation of fluid behavior for the chosen flow fields and a dominant southerly flow. The specific functions in the program that address the movement of particles are called *Move*, *MoveQuant*, and *Barrier*.

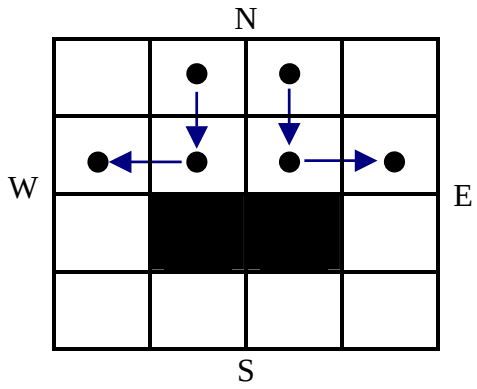

Figure 2-3. Two particles (black circles) encountering a barrier while moving south. The particle on west side of the barrier moves to the west, and the particle on the east side moves to the east.

For each particle that is moved to grid point (i, j), the number of particles at grid point (i, j) is incremented by one, and after each time step a new distribution of particles over the flow field is established. Simultaneously, a matrix of flows is generated, which increments by one the number of transfers from grid point (i, j) to grid point (k, l). After each time step a complete flow matrix is available for calculating the network indices.

The program generates five output files in text format (Table 3) that describe the development of the flow field after each time step.

Table 3. Output files from the cellular automata program.

Name	Description
filename.txt.BIOM.txt	Stores the number of particles at each grid point after each time step. BIOM = biomass (a holdover from the original ecosystem focus).
filename.txt.AMI.txt	Stores the network AMI after each time step.
filename.txt.ASC.txt	Stores the contribution of each grid point to the overall network ascendency (i.e. A_j) after each time step.
filename.txt.SAsc.txt	Stores the sensitivities of A to each flow f_{pq}.
filename.txt.OUT.txt	Stores the number of particles transferred from each grid point (i, j) to its four neighbors after each time step.

The output from each file is discussed in the Results section below.

The f.. remains constant and may be calculated before any movement of particles takes place, because every particle is required to move once (and only once) during each time step, and there are no external transfers. For a 20 x 20 grid without barrier grid points and 100 particles initially distributed at each grid point, the f.. = 40,000. Calculating the AMI after each time step is accomplished by the *AMICalc* function (Figure 2-4). The flow matrix storing all transfers between grid points after each time step is referred to as `Out3D` in the code.

```
1.    int AMICalc(int s)  //for each timestep s
2.    {
3.      gsl_vector * SC; //define two pointers to vectors, where
C=column and R=row and S=sum
4.      gsl_vector * SR;
5.      double tmpAMI, tmp2, tij;
6.      int i, j;
7.      SC=gsl_vector_calloc(N*N);   //allocate vectors as N*N and
initialize to zero
8.      SR=gsl_vector_calloc(N*N);
9.      for (i=0; i<(N*N); i++)
10.     {
11.       for (j=0;j<(N*N);j++)
12.       {
13.         gsl_vector_set(SC,j,gsl_vector_get(SC,j)+gsl_matrix_get(Out
```

```
3D,i,j));   //sets the jth element of vector SC to be itself + the
value in Out3D (i, j).  Sum all j's, i.e. all columns in row i
14.         gsl_vector_set(SR,i,gsl_vector_get(SR,i)+gsl_matrix_get(Out
3D,i,j));   //sets the ith element of vector SR to be itself + the
value in Out3D (i, j).  Sum all i's, i.e. all rows in column j
15.       }
16.     }
17.     tmpAMI=0;
18.     //scan the matrix for Tij >0
19.     for (i=0; i<(N*N); i++)
20.     {
21.       for (j=0;j<(N*N);j++)     //look at every tij in the Out3D
flow matrix
22.       {
23.         tij=gsl_matrix_get(Out3D,i,j);      //if the transfer
between cells is not 0...
24.         if (tij!=0) //if the transfer is 0, then it does not
contribute to the AMI
25.         {
26.           tmp2=gsl_vector_get(SC,j)*gsl_vector_get(SR,i);
              //...then calculate the denominator in the log () term of
the AMI
27.           if (tmp2!=0)
28.           {
29.              tmpAMI=tmpAMI+(tij/TST)*log(tij*TST/tmp2); //calculate
the AMI for one tij and store it as tmpAMI, and continue summing for
all tij, so that once
30.   //the loops are done tmpAMI = AMI.
31.           }
32.          }
33.       }
34.     }
35.   gsl_vector_set(AMI,s,tmpAMI);       //for each time step s, set
the sth element in the vector AMI to be tmpAMI
36.   return 0;
37.   }
```

Figure 2-4. Code written in C for calculating the AMI after each time step in the cellular automata program. Adapted from Allesina (2004).

In lines 13-14 the function defines two vectors SC and SR as the sums of all transfers in column *j* and row *i*, respectively, of the flow matrix at time step *s*. Vector SC is equivalent to the quantity T_i. and vector SR is equivalent to the quantity $f._j$ in the log term of (1.7) for the AMI. For every non-zero transfer between grid points, the variable `tmp2` stores the product of SC and SR, and is subsequently used to calculate a running

summation of the AMI after each time step *s*. Plots of the AMI after each time step for the three flow fields are discussed in the Results section.

Since A = (AMI) (f..) and f.. is a constant, plotting A after every time step provides no additional information about the organization of the flow field not already discernable in the plots of the AMI after each time step. Of greater interest is the distribution of the ascendency over the flow field plotted by calculating the contribution of each grid point to the total A, as described in (2.1). The function performing this calculation following each time step is *AscCalc* (Figure 2-5).

```
int AscCalc(void)
{
int i, j;
double fij, Aj;
gsl_vector * SumC;     //*SumC = column sum pointer to the vector SumC
SumC=gsl_vector_calloc(N*N);

//Divide every flux by the f.. and compute the entropies

//Preserve the flows in StoreSAsc for calculating the sensitivities
later
gsl_matrix_memcpy(StoreSAsc,Out3D);

for(i=0;i<N*N;i++)
{
     for(j=0;j<N*N;j++)     //for every element in the flow matrix...
     {
//Aj=fij log(fij*TST/MiMj)       //this formula refers to the A(j)
formula which calculates the contribution of each cell in the flow
field to the network ascendency
          fij=gsl_matrix_get(Out3D,i,j);   //temporarily store the value
of each element in the flow matrix
          if (fij>0)    //just analyze non zero transfers
          {   //The product is Mi*Mj

     tmp=gsl_matrix_get(M,(int)i/N,i%N)*gsl_matrix_get(M,(int)j/N,j%N)
               //if the # particles at (i/N, i%N) * the # particles at
(j/N, j%N) is greater zero, then…
                if (tmp!=0)
               {
                    Aj=fij*(log((fij*TST/tmp));
                    //...calculate the Aj for that flow and store as Aj
```

```
                    gsl_matrix_set(Out3D,i,j,Aj);    //...store the
temporary Aj values in the Out3D matrix

     gsl_vector_set(SumC,j,gsl_vector_get(SumC,j)+gsl_matrix_get(Out3D,i
,j));
//Sum over all rows to calculate the total contribution of each cell to
A.  To calculate the overall A I would sum over all rows and columns
                }
           }
     }
}
for (j=0;j<N*N;j++)
{
     gsl_matrix_set(AscComp,(int)j/N,j%N,gsl_vector_get(SumC,j)); //Fill
the matrix AscComp with the values from SumC
}
return 0;
}
```

Figure 2-5. Code written in C for calculating the A_j after each time step in the cellular automata program. Adapted from Allesina (2004).

The *AscCalc* function, first excludes every non-zero flow, and then calculates the product of the quantities M_i and M_j, which represent the number of particles (or mass) in the particle matrix, M, at grid points *i* and *j* respectively. Since this product is the denominator in the $\log_2$ term of (2.1), a check is made to ensure no division by zero occurs. The contribution to the ascendency made by each individual flow, f_{ij}, is stored in the N^2 x N^2 matrix *Out3D*. The vector *SumC* of length N^2 is used to store the summation of all rows, *i*, as is required in calculating A_j (2.1). Once all flows occurring after time step *s* are accounted for, the values in *SumC* are transferred to the global N x N matrix *AscComp*, which is referenced when plotting the distribution of the ascendency over the flow field.

The code for calculating the sensitivities of the ascendency to individual flows is very much the same as the code just described above for calculating the contribution of each flow, f_{ij}, to the overall ascendency. Given the similarity, the code for calculating the

sensitivities is not reproduced in the text. Comparing the equations for the ascendency (1.8) and the sensitivities (1.9) should reveal that the sensitivities to the overall ascendency are represented by the logarithm term in (1.8).

2.2. Results from the Cellular Automata Method

As was shown with a simple four-compartment network in Chapter 1, a higher AMI indicates that the represented systems transfer medium among their constituent components with greater order or organization than networks with a lower AMI. One could also say that systems with a lower AMI are more stochastic or disorganized in the manner in which they transfer medium. The same reasoning is applied to the three flow fields described in the previous sections of this chapter using the AMI as the criteria for comparing the flow fields.

Results are presented for three flow field examples: 1) a flow field without obstruction to the flow, 2) a flow field where flow is perpendicular to an impermeable barrier located in the center of the flow field, and 3) a flow field where flow through a channel redirects particles into the center of the flow field. The examples are referred to as “free,” “barrier,” and “channel,” respectively. The grid points that make up the obstruction within the barrier flow field are highlighted in green, and those making up the obstruction in the channel flow field are highlighted in red (Figure 2-1). All five scenarios summarized in Table 2.1 were run for each flow field example.

2.2.1 The free flow field—flow without obstruction

In the free flow field, the AMI comes to equilibrium almost immediately with all five scenarios (Figure 2-6).

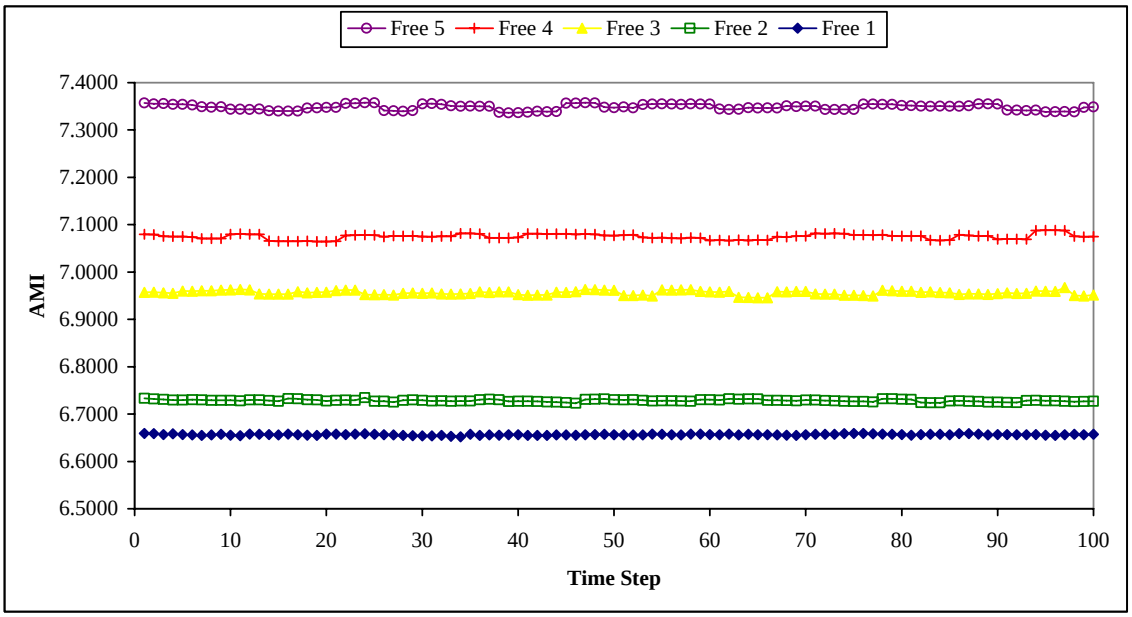

Figure 2-6. AMI after each time step for the five scenarios (labeled Free 1—Free 5 on the graph) applied to the free flow field. For all cases the AMI reaches an equilibrium immediately, and increases as the probability of directional flow to the south increases.

Increasingly greater constraint is imposed on the flow with each successive scenario (labeled Free 1 through Free 5 in the graph) and, as anticipated, the AMI increases correspondingly, signifying that the flow becomes more organized in each case. By analogy, with the simple four-compartment network, the maximally connected and minimally organized network is generated by scenario #1 (labeled "Free 1" in the legend), and the most highly organized network in this example is generated by scenario #5. The maximally organized case, which would have required all particles to move in

one and only one direction was not applied because, particularly in the barrier and channel flow fields, moving particles in such a restrictive way would certainly have not mimicked the motion of a fluid.

2.2.2 The barrier flow field

A barrier perpendicular to the dominant direction of flow is added to the free flow field by preventing particles from accessing eight centrally located grid points. The barrier grid points are those bounding cells 190, 191, and 192 (Figure 2-1), and are henceforth collectively referred to as the barrier. The following rules apply when a particle encounters the barrier:

1) If the particle is on the western half of the barrier and is moving either north or south, it is directed to move west.
2) If the particle is on the eastern half of the barrier and is moving either north or south, it is directed to move east.
3) If a particle is moving east it is directed to move west.
4) If a particle is moving west it is directed to move east.

The general purpose of the rules is to maintain a continuity of flow following interaction with the barrier.

Applying these rules and the homogenous directional assignments in scenario #1 to the barrier flow field results in a uniform distribution of particles over the flow field with only slight peaks adjacent to the barrier grid points (Figure 2-7).

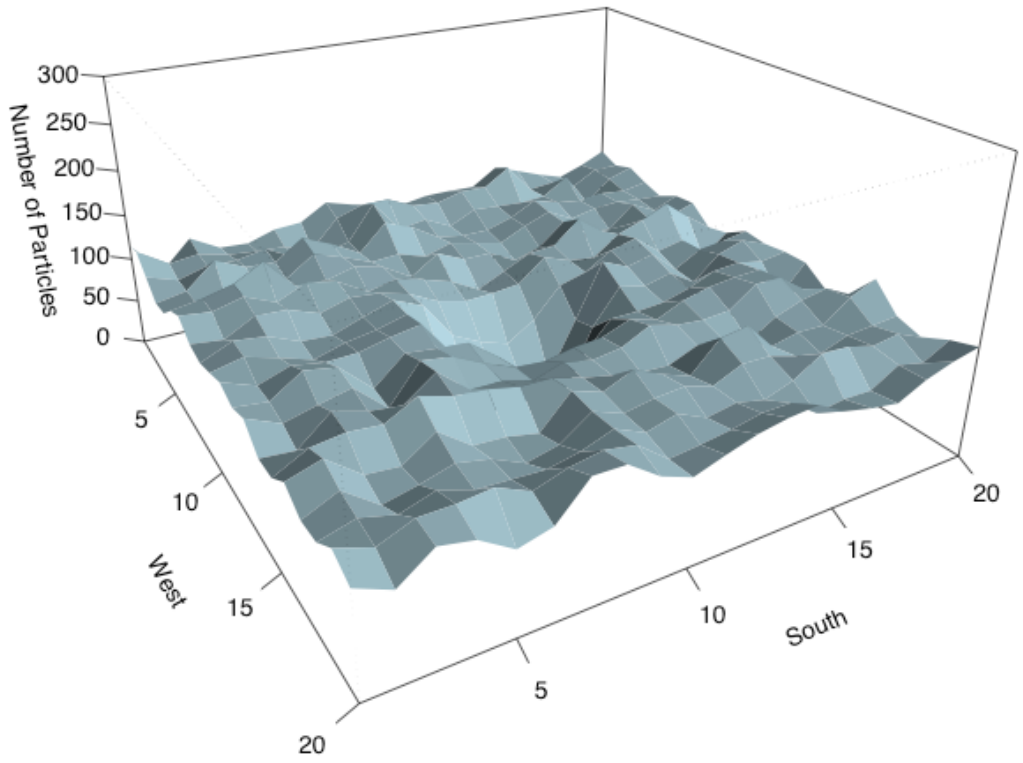

Figure 2-7. Distribution of particles across the barrier flow field after 100 time steps and with the pseudo random directional assignments of scenario #1. The values on the z-axis represent the number of particles at each grid point.

Introducing a southerly bias to the flow changes the distribution of particles over the flow field. Applying the directional assignments of scenario #3 increases the probability that a particle will move south at each time step from 25% to 46%. After only five time steps an accumulation of particles just upstream and at the ends of the barrier is evident (Figure 2-8a). After 40 time steps, the accumulation peaks are obvious and a minimum in the distribution of particles is obvious on the downstream side of the barrier (Figure 2-8b). After 100 time steps the distribution has reached an equilibrium, with a relatively constant number of particles accumulating just beyond the barrier ends, and a well

developed minimum on the downstream side of the barrier that nearly reaches the far-field level before wrapping around to the northern end of the flow field (Figure 2-8c).

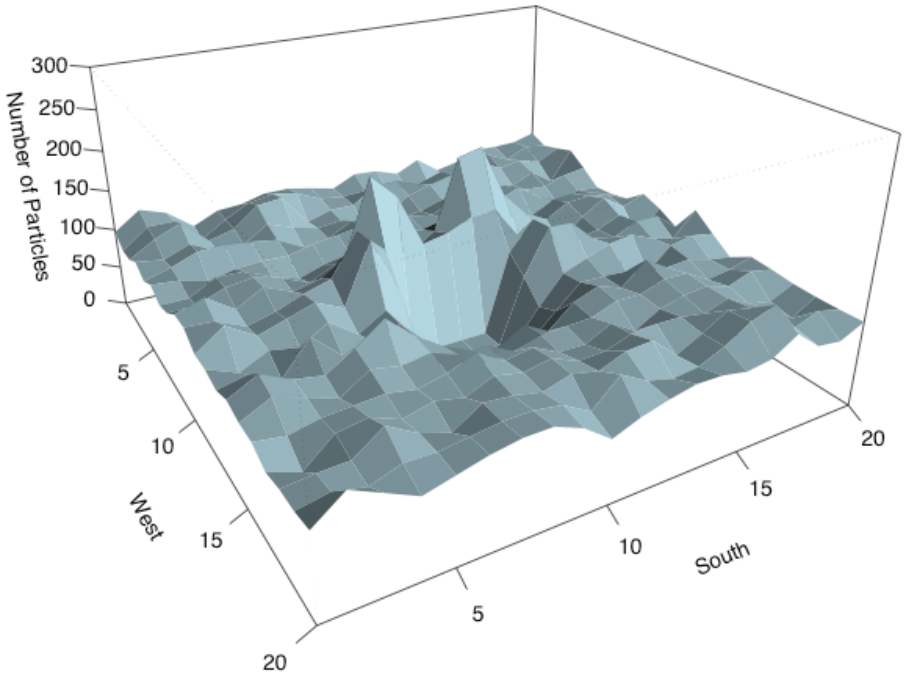

a

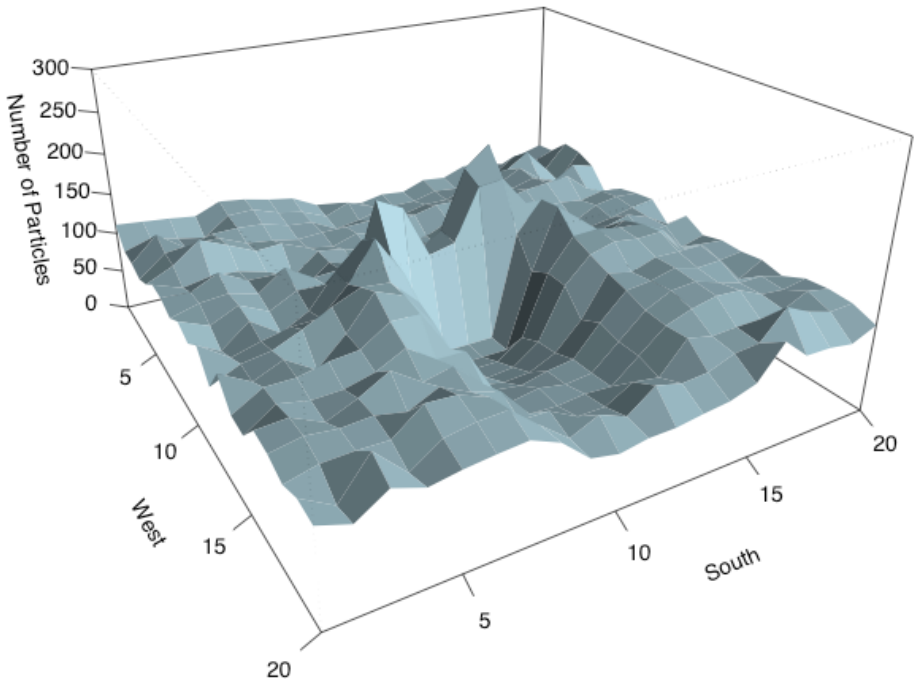

b

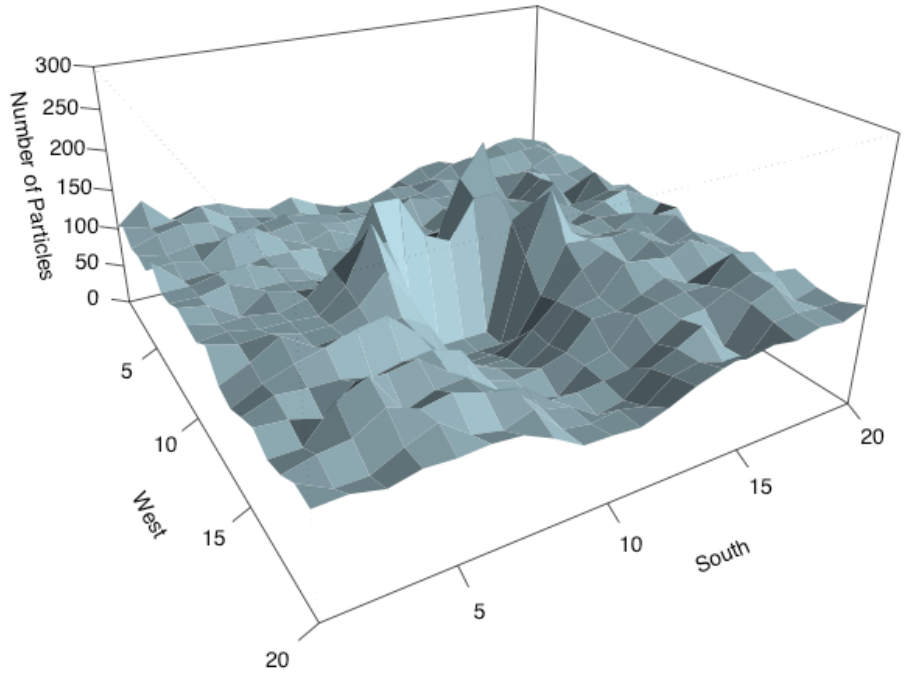

c

Figure 2-8. Development of the barrier flow field subject to the directional assignments of scenario #3 after a) 5 time steps, b) 40 time steps, and c) 100 time steps.

These results agree reasonably well with those from the ecological landscape study by Ulanowicz (2000), which applied a similar cellular automata method.

The organization of the flow field following the introduction of a barrier is measured in the same way as the organization of flow without a barrier. The AMI of the barrier flow field increases as the probability of flow to the south increases (Figure 2-9), in much the same way as with the free flow field.

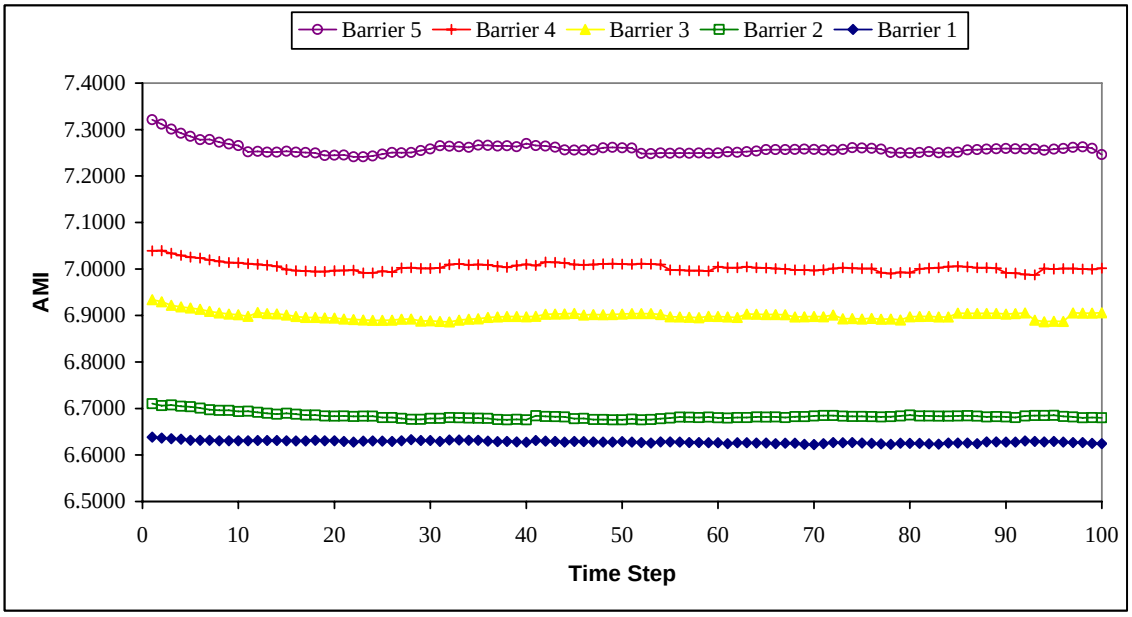

Figure 2-9. AMI after each time step for the five scenarios (labeled Barrier 1—Barrier 5 on the graph) applied to the barrier flow field. For all cases the AMI reaches an equilibrium after about 30 time steps, and increases as the probability of directional flow to the south increases.

A slight decline in the AMI over the first ten time steps is noticeable in each of the curves representing scenarios #2 through #5. This adjustment to the AMI is undoubtedly caused by the introduction of the barrier. The addition of barrier grid points reduces the number of possible pathways within the flow field and decreases the f.. relative to the f.. of the free flow field. The AMI of the barrier flow field reaches equilibrium before 30 time steps for all five scenarios.

The network ascendency, A, can be calculated after each time step in the same way the AMI is calculated. However, because the networks studied here are closed and all particles move once at each time step, f.. remains constant throughout. Recalling that A = (f..)(AMI), should convince the reader that plots of A after each time step will simply be scaled versions of the ones above.

In order to better visualize the dynamics of the flow, the ascendency is plotted over the full flow field by summing over only one index (2.1). Three-dimensional plots showing the contribution of each flow, f_{ij}, in the flow field to the overall ascendency reveal that regions of greater activity (i.e. larger flows) appear to have a proportionately greater effect on the overall development of the flow field (Figure 2-10). These are also the same regions most affected by the constraints (i.e. the barrier grid points) in the flow field. Intuitively it makes sense that A, which is a combination of both f.. (activity) and AMI (information, or alternatively, constraint), increases as both of those attributes increase. Regions in a flow field that provide the greatest contribution to the overall network ascendency are the same regions which have the greatest influence on the development of the flow field over time. In terms of characterizing the flow, the regions making the greatest contribution to the overall ascendency are interpreted as control points or "bottlenecks" in the flow.

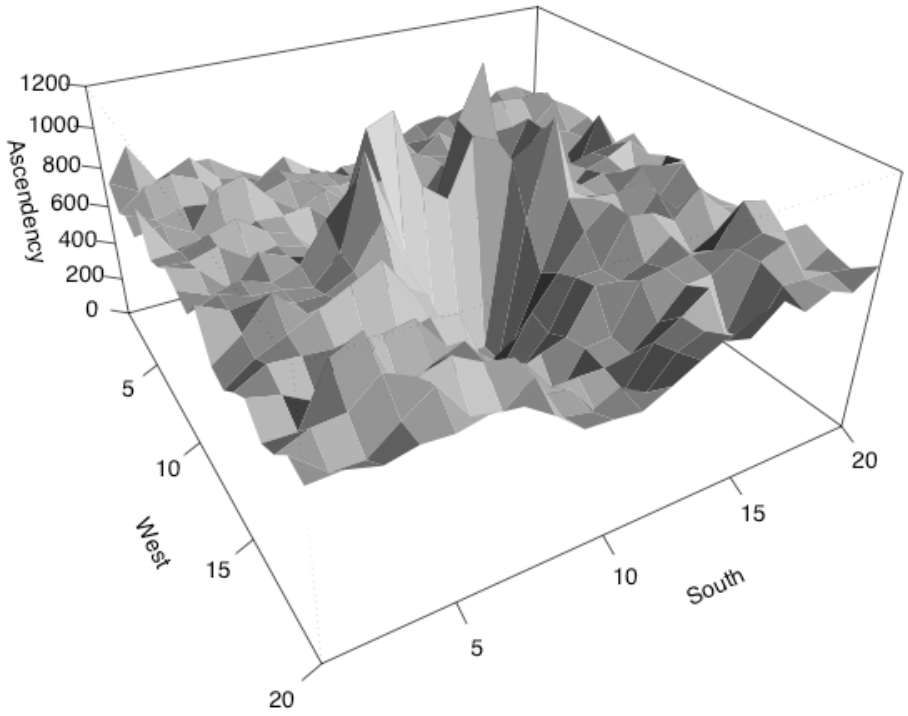

Figure 2-10. Contour plot of the contribution at each point in the barrier flow field to the overall network ascendency. Values for A are generated after 100 time steps and under the conditions defined by scenario #3.

Comparable results are achieved with the assignments of scenarios #2, #4, and #5. With each scenario, the same regions in the flow field display maximum and minimum values both in the number of particles and in the ascendency (Figure 2-11). As the probability of southerly flow increases, the development of maxima and minima in the flow field occur more rapidly.

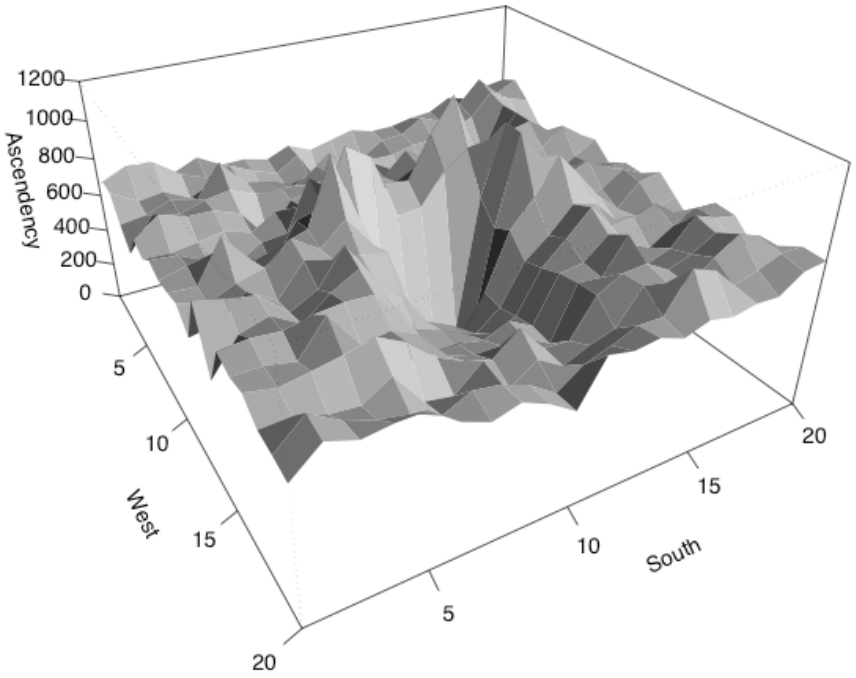
Ascendency
1200
1000
800
600
400
200
0
West
5
10
15
20
South
5
10
15
20

a

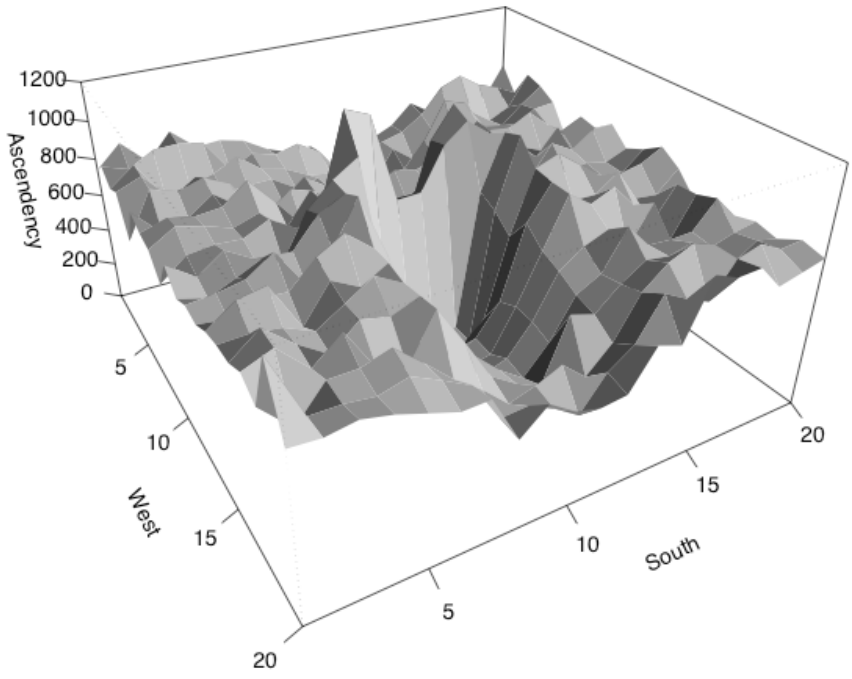
Ascendency
1200
1000
800
600
400
200
0
West
5
10
15
20
South
5
10
15
20

b

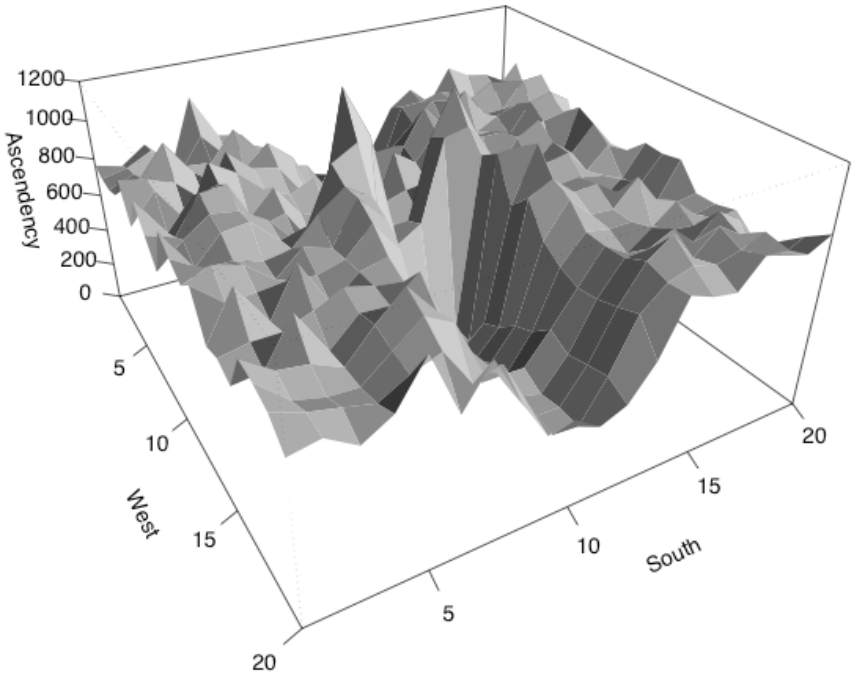

c

Figure 2-11. Contour plots of the contribution at each grid point in the barrier flow field to the overall network ascendency. Values for A are generated after 100 time steps and under the conditions defined by scenarios a) #2, b) #4, and c) #5.

The sensitivity of the ascendency to individual flows is calculated according to (1.9). Just as with the contributions to the ascendency, the sensitivities are distributed over the flow field but instead highlight those areas exhibiting the greatest amount of resistance to flow (Figure 2-12). Comparing the distribution of the ascendency (Figure 2-11) with the distribution of the sensitivities reveals that the areas of the flow field with the least amount of ordered activity (i.e. the lowest values in Figure 2-11) have the highest sensitivity values (i.e. the peak values in Figure 2-12). Pathways of greatest activity are highlighted by the ascendency, and pathways of greatest resistance are highlighted by the sensitivities. The highest sensitivity values (Figure 2-12) appear on the downstream side of the barrier; the pathways in the flow field where the fewest number of particles transit, and where the fewest flows, f_{ij}, occur. By highlighting

inactivity the sensitivities reveal disturbances in the flow, in this case the presence of the barrier, that might be obscured by the flows in a more complex flow field.

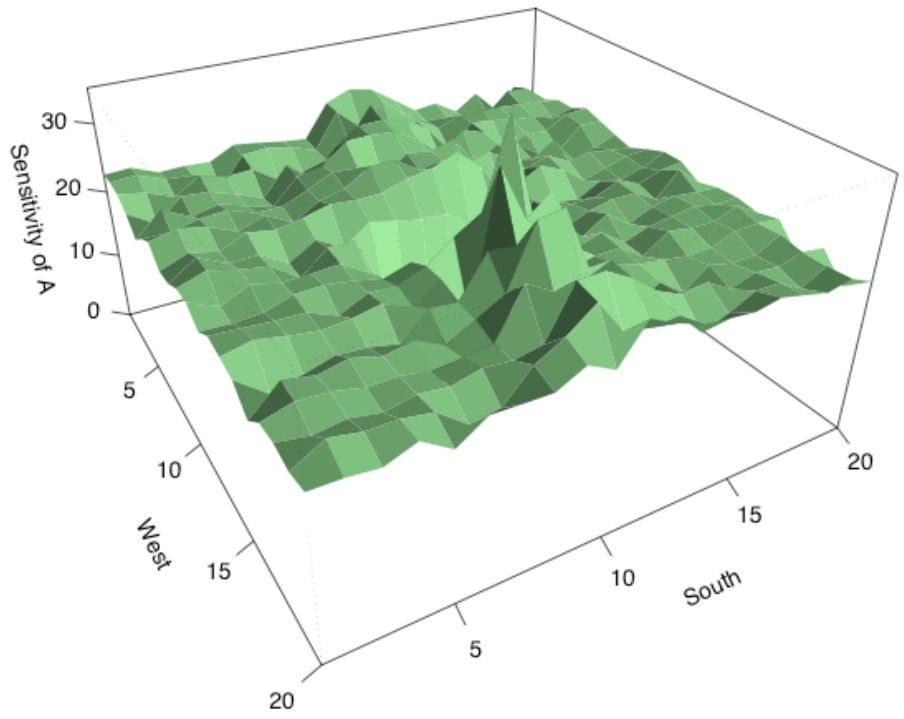

Figure 2-12. Sensitivities of the overall ascendency to individual flows in the barrier flow field. Data are plotted after 100 time steps and with the directional assignments of scenario #5.

2.2.3 The channel flow field

A channel is formed in the free flow field by reassigning the eight barrier grid points to the eastern and western edges of the flow field (Figure 2-1). The grid points are collectively referred to as the channel walls. Particles encountering a channel wall are directed towards the center of the flow field according to the following rules:

1) If the particle is on the western half of the flow field and is moving either north or south, it is directed to move east.
2) If the particle is on the eastern half of the flow field and is moving either north or south, it is directed to move west.
3) If a particle is moving east it is directed to move west.
4) If a particle is moving west it is directed to move east.

As in the barrier example, the approach in defining rules is to maintain a continuity of flow.

Applying these rules and the assignments in scenario #1 to the channel flow field results in a uniform distribution of particles over the flow field, with only small peaks adjacent to the channel walls (Figure 2-13).

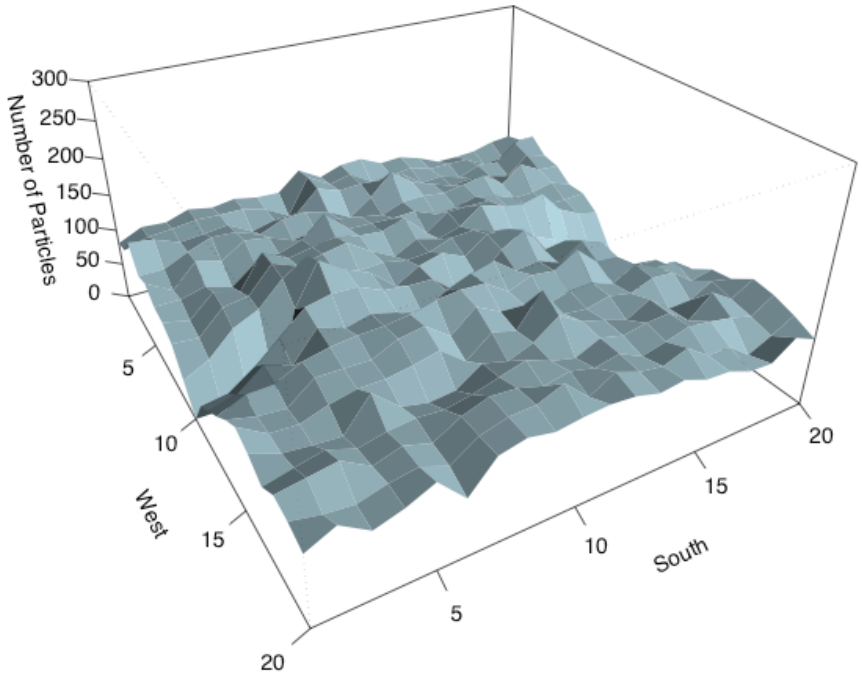

Figure 2-13. Distribution of particles across the channel flow field after 100 time steps and with the pseudo random directional assignments of scenario #1. The values on the *z*-axis represent the number of particles at each grid point.

Introducing a southerly bias to the flow changes the distribution of particles over the flow field. Applying the directional assignments of scenario #3 increases the probability that a particle will move south at each time step from 25% to 46%. After three time steps, an accumulation of particles on the upstream side of the channel walls is observed with more particles accumulating towards the center of the flow field (Figure 2-14a). After thirty time steps, maxima in the number of particles are established just beyond and upstream of the ends of the channel walls, and obvious minima are observed on the downstream side of the channel walls (Figure 2-14b). After 100 time steps the distribution has reached an equilibrium, with a relatively constant number of particles accumulating just beyond the channel walls, and well developed minima on the downstream side of the channel walls (Figure 14c).

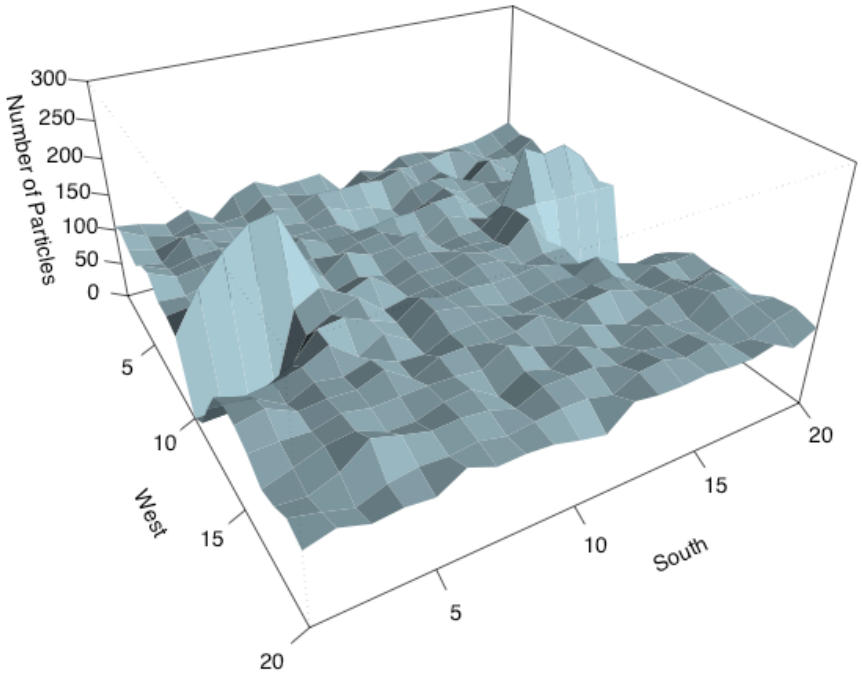
Number of Particles
300
250
200
150
100
50
0
West
5
10
15
20
South
5
10
15
20

a

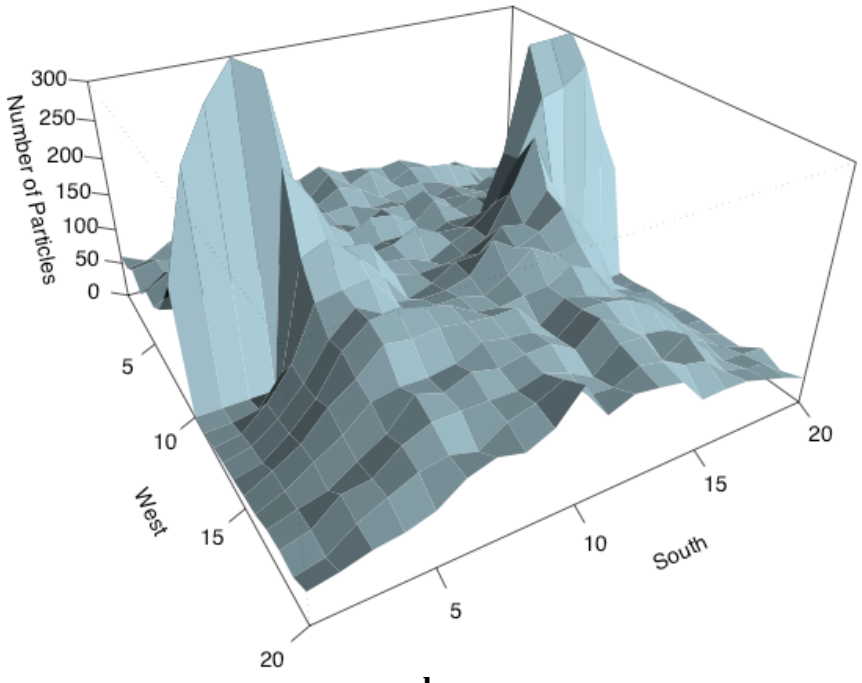
Number of Particles
300
250
200
150
100
50
0
West
5
10
15
20
South
5
10
15
20

b

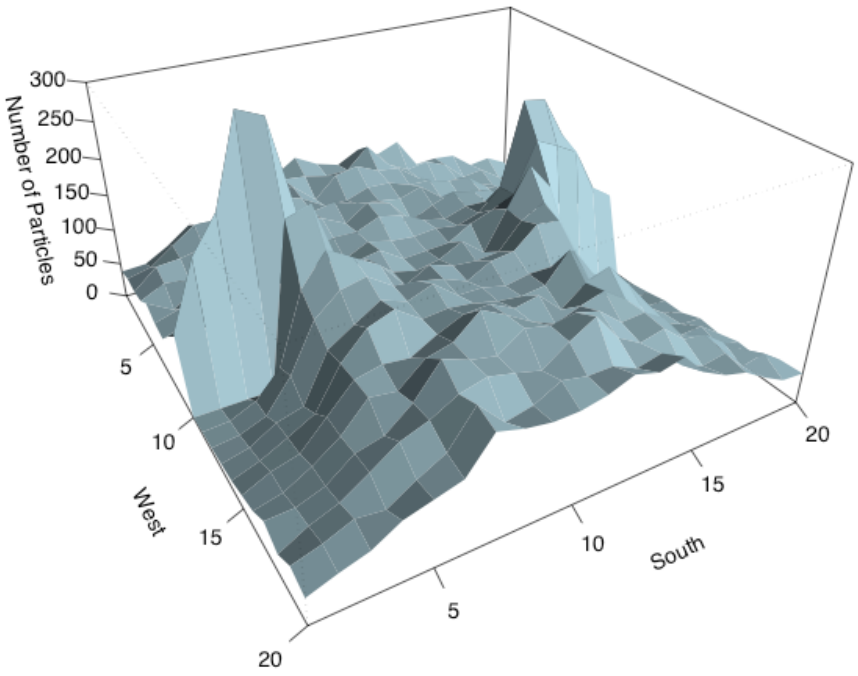

c

Figure 2-14. Distribution of particles across the channel flow field after 1) 3 time steps, b) 30 time steps, and c) 100 time steps and subject to the conditions of scenario #3. The values on the *z*-axis represent the number of particles at each grid point.

A majority of particles remains within the channel after being redirected towards the center following an encounter with a channel wall. This is particularly the case with scenarios #4 and #5, because once a particle moves into the center of the flow field where it is able to move south without encountering a channel wall, the probability that it continues south is 56% and 68% respectively. The effect is that very little diffusion occurs to the east or west, and therefore increasingly fewer particles encounter the channel walls, so that the maximum number of particles occurring at the peak locations decreases over time. This fluctuation in the number of particles at the peak locations is best observed by displaying the plots in succession from time step 1 to 100 as a movie. However, evidence of the phenomenon is also evident in a comparison of the peak locations after 30 and 100 time steps (Figure 2-14b and c)

The AMI of the channel flow field does not reach equilibrium until after 65 time steps for all five scenarios, and the distinction between the equilibrium AMI of scenario #1 and that of scenario #2 is negligible (Figure 2-15). The difference in the organizational development, as measured by the AMI, between the channel and barrier flow fields is attributable to the distribution of the eight barrier grid points across each flow field (Figure 2-1). All eight grid points in the channel flow field directly impede flow to the south, whereas only four grid points are directly exposed to southerly flow in the barrier flow field. Additional experiments varying the number of blocked grid points in a flow field directly influenced the number of time steps required before the AMI of the flow field reached equilibrium. In general, the fewer the number of grid points, the faster equilibrium was achieved.

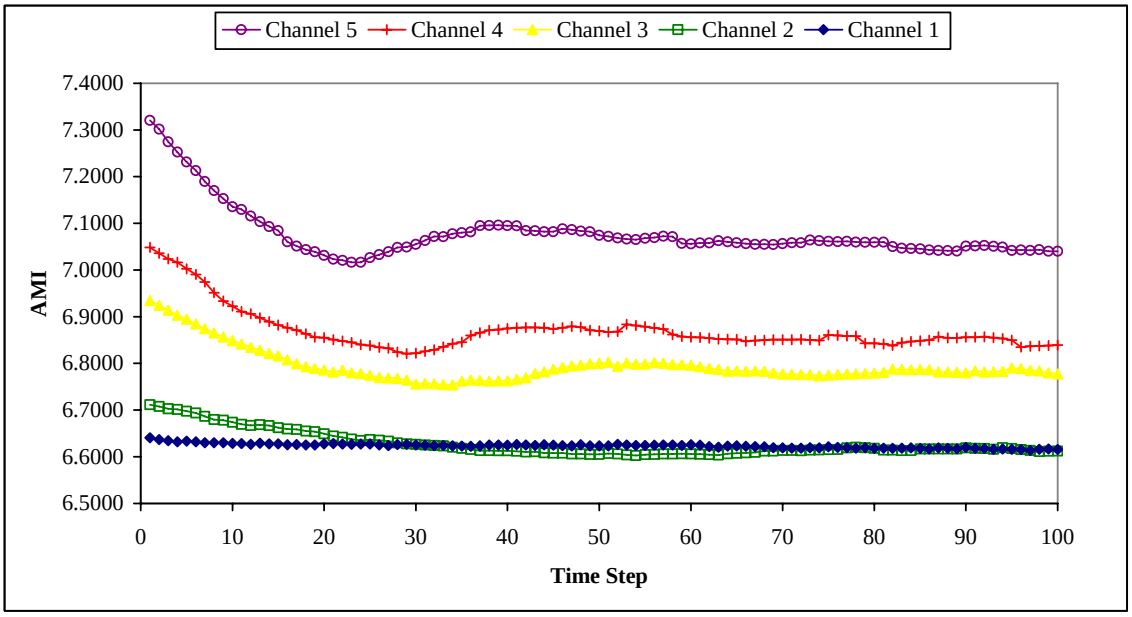

Figure 2-15. AMI after each time step for the five scenarios (labeled Channel 1—Channel 5 on the graph) applied to the channel flow field. For all cases the AMI reaches an equilibrium after about 60 time steps, and increases (although by an insignificant amount between 1 and 2) as the probability of directional flow to the south increases.

A more pronounced transient decay of the AMI (than was observed in the barrier flow field) is displayed over the initial time 30 steps for scenarios #2 through #5. As in the barrier flow field, the decline is an adjustment to the artificially high AMI calculated after the first time step, when all particles have moved once according to the prescribed probabilities, and few have encounter the channel walls.

Consistent with the results from the barrier flow field, the contribution of each flow, f_{ij}, to the overall ascendency of the channel flow field reveals that regions of greater activity (i.e. larger flows) appear to have a proportionately greater effect on the overall development of the flow field (Figure 2-16).

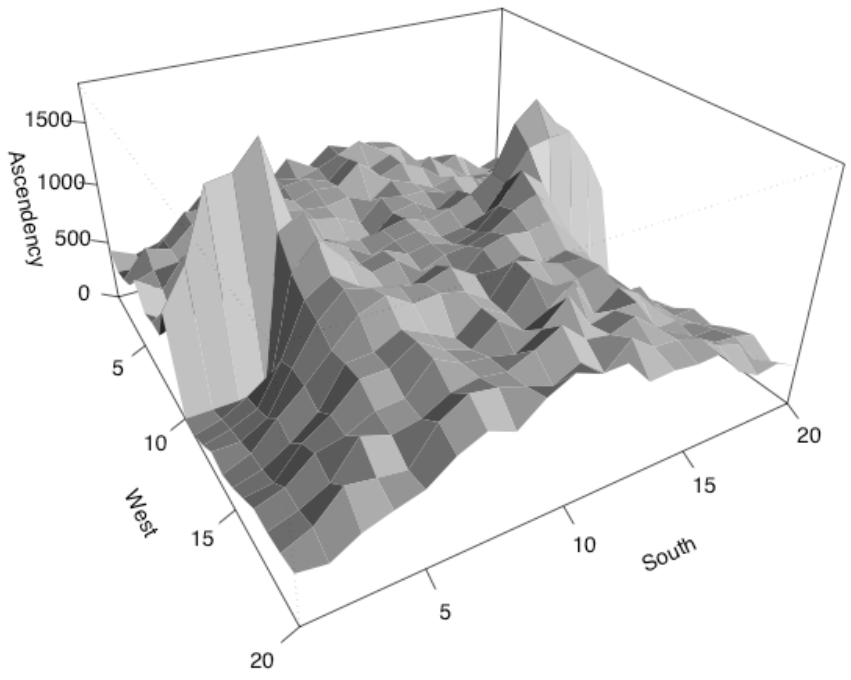

Figure 2-16. Contour plot of the contribution at each point in the barrier flow field to the overall network ascendency. Values for A_j are generated after 100 time steps and under the conditions defined by scenario #3.

Regions of the flow field exhibiting the least amount of ordered activity are highlighted by the sensitivity of the ascendency to individual flows (Figure 2-17). Alternatively, one might describe these flows as the pathways of greatest resistance to the overall flow. In the channel flow field, the ascendency is most sensitive to changes in the flows occurring immediately upstream and downstream of the barrier grid points located at the eastern and western extremes of the flow field. As in the barrier flow field, areas downstream of the barrier grid points are those to which the ascendency is most sensitive and are those which exhibit the least organized activity. Peaks in the sensitivity of the ascendency located in the northeastern and northwestern corners of the flow field are artifacts associated with the wrap-around boundary conditions.

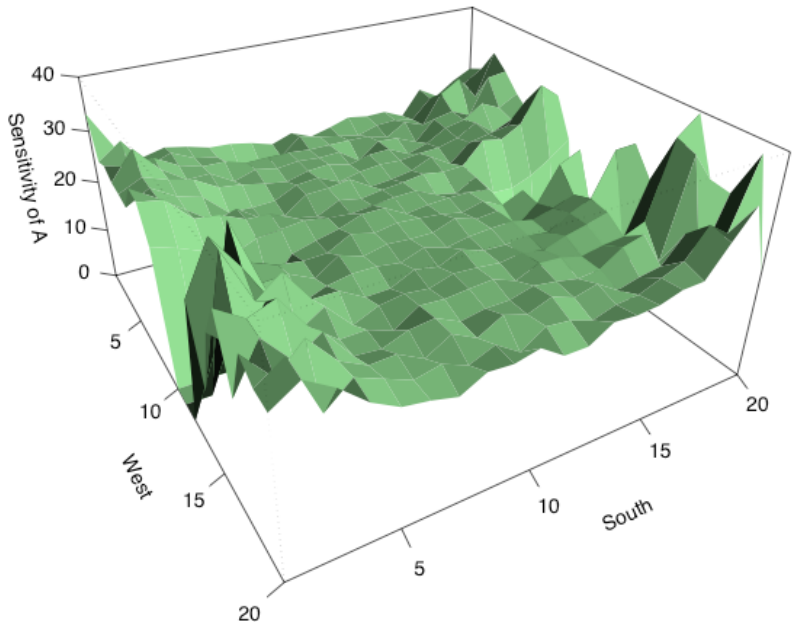

Figure 2-17. Sensitivities of the overall ascendency to individual flows in the channel flow field. Data are plotted after 100 time steps and with the directional assignments of scenario #5.

2.2.4 Comparison of the three flow fields

As was done for the four-compartment network in Chapter 1, values for the network indices f.., AMI, and A for each flow field example are calculated (Table 4). In the free flow field, an increase in the probability of flow to the south from 25% to 68% added 0.6919 bits of information to the organization and 27,675 flow bits of ascendency to the dynamics of the system. The same adjustment in the flow applied to the barrier flow field added 0.6283 bits of information and 24,631 flow bits of ascendency to the system. In the channel flow field the organization increased by 0.6207 bits of information and the dynamics increased by 24,331 flow bits of ascendency.

Table 4. Index values for the free, barrier, and channel flow fields subject to the five flow scenarios. AMI values are averages taken after the time step at which equilibrium is achieved in each example. A is calculated as the product of f.. and AMI.

Flow Field	Scenario	Network Index		
		f.. (flow units)	AMI (bits)	A (flow bits)
Free	1	40,000	6.6565	266,259
	2		6.7286	269,145
	3		6.9562	278,246
	4		7.0750	283,000
	5		7.3484	293,934
Barrier	1	39,200	6.6274	259,795
	2		6.6809	261,893
	3		6.8974	270,378
	4		7.0020	274,476
	5		7.2558	284,426
Channel	1	39,200	6.6235	259,641
	2		6.6912	262,294
	3		6.7948	266,355
	4		7.0254	275,395
	5		7.2442	283,972

Plots of the contribution to the ascendency are unremarkable in the free flow field, because without any obstacles to redirect flow each cell in the flow field contributes about equally to the overall system ascendency. This is not the case for the barrier and channel flow fields (Figure 2-11, Figure 2-16). In both examples, cells that are both adjacent to the barrier cells and exposed to the regions of free flow contribute most to the overall ascendency, and are therefore critical to the development of each flow field.

A seemingly obvious conclusion to draw from a comparison of the three flow fields is that adding barriers to a flow *decreases the organization*, or ordered flow, through a flow field. For each scenario, the ascendency of the free flow field is greater

than the barrier flow field, which in turn is greater than the channel flow field. This trend contradicts the results achieved by Ulanowicz (2000), who reported a slight increase in the AMI with the insertion of a barrier impeding the flow. However, a key distinction and the likely explanation for this discrepancy is that an increase in the f.. is reported by Ulanowicz (as an artifact) with the inclusion of a barrier, and a decrease in the f.. occurs in the examples just presented.

2.2.5 Fluid-like behavior

As the probability of moving to the south increases in the barrier flow field, the particles are induced to move around the barrier in much the same way a fluid, subject to an increase in flow rate, would move around a similar barrier in an actual flow field (Batchelor 1970). Other models of two-dimensional flow where obstacles are inserted into the flow field have yielded similar patterns (Pozrikidis 1999).

Comparing the results from scenarios #2, #4, and #5 for the channel flow field after 60 time steps highlights this fluid-like behavior of the particles (Figure 2-18). With a probability of flow to the south at 36% (Figure 2-18a), the flow field is characterized by peaks at the inner edge and just upstream of the channel opening and slight ridges that form downstream of the peaks. The ridges diffuse almost completely before the particles wrap around to the northern end of the flow field. With the probability of flow to the south at 46% (Figure 2-18b), the particles build up more rapidly at the same peak locations as they try to circumvent the side barriers and have less opportunity to diffuse,

resulting in a greater channeling of the particles. This behavior is analogous to a fluid moving through a channel at an initial rate, and then having the flow increased to a greater rate. The effect is even more pronounced when the probability of movement to the south increases to 68% (Figure 2-18c). Here very little time is left for diffusion to the east and west as the fluid is propelled through the opening.

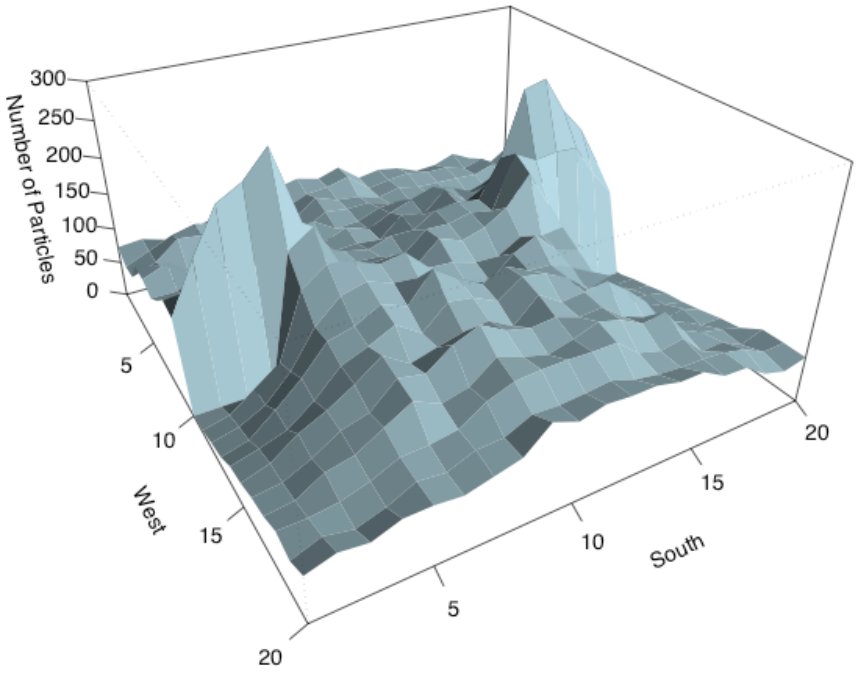

a

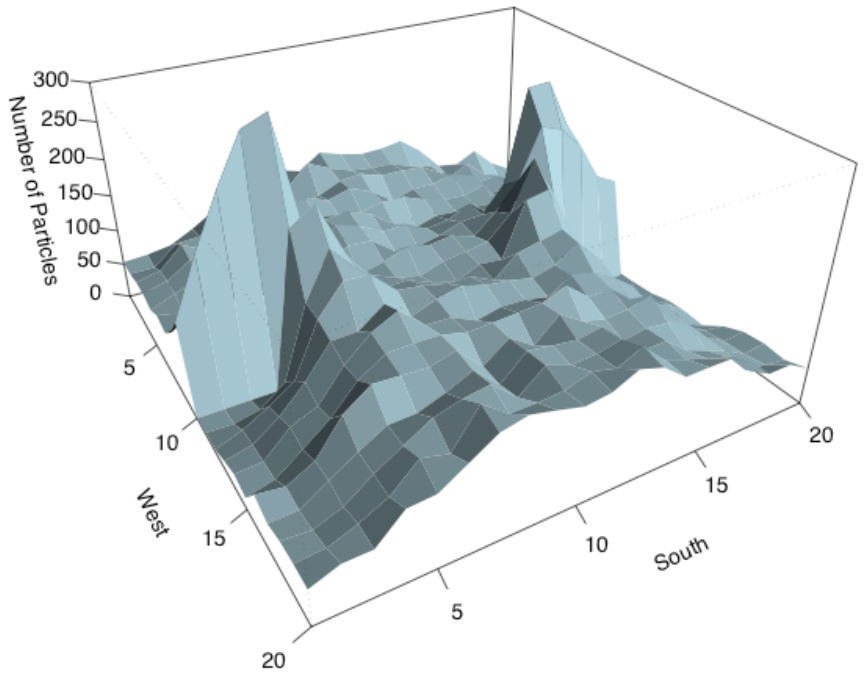

b

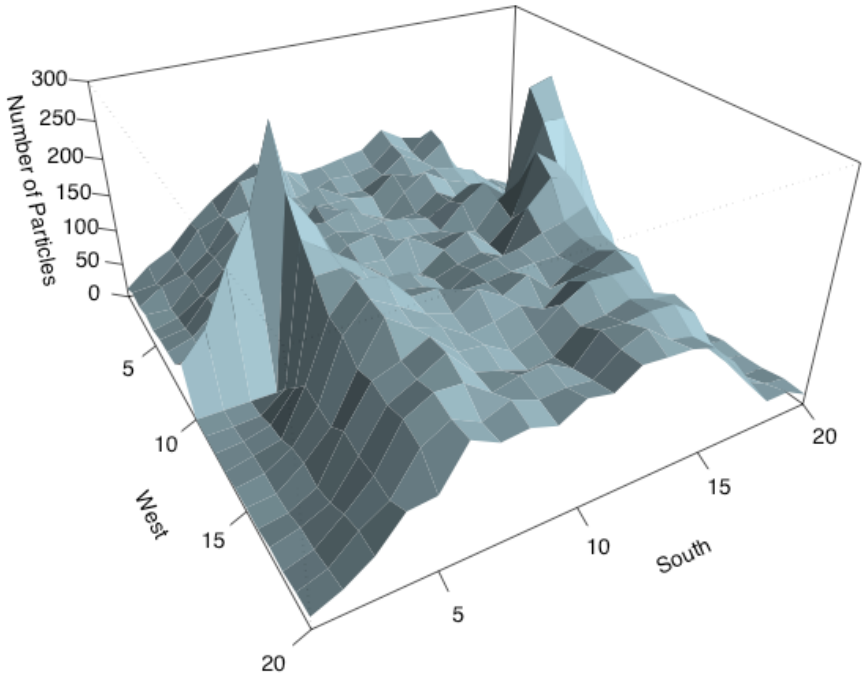

c

Figure 2-18. Movement of particles through a channel after time step 60 for the conditions given in a) scenario #2, b) scenario #3, and c) scenario #5. The resulting flow patterns exhibit characteristics of a fluid subject to increasing rates of flow.

2.2.6 Connectance

Another means of characterizing a network of flows is to describe its structure in terms of the network connectance. The connectance is the average number of connections, or flows, initiating from each grid point within the network. The connectance, like the AMI, varies with every time step. In the free flow field, every grid point exchanges flows with at least one other grid point but no more than four grid points. Therefore, the number of connections in a representative network must be between N (unlikely) and 4N (more likely). As directional flow strengthens, the distribution of flows among these connections also varies, so that calculating an "effective connectance" (Zorach and Ulanowicz 2003) is another way of describing a network.

Chapter 3: Analytical Examples from Fluid Dynamics

Four well understood analytical examples from the field of fluid dynamics are modeled and represented as networks. These examples were chosen because they are relatively simple to model and because the characteristics and behavior of the flow will be familiar to fluid dynamicists and physical oceanographers for whom the results of this research have the greatest potential benefit. All four examples are adapted from descriptions found in Bird et al. (1960), and unless otherwise stated, any additional information desired by the reader should be available in that reference.

3.1 Analytical examples of fluid flow

A flow, f_{ij}, within the flow matrix is determined by calculating the integral along a line connecting two grid points. The result of the integration is essentially the average flow occurring between two grid points. For laminar flow in the x-direction with velocity, V(x), defined at each grid point (a, b) the flow, $f_{i-1,i}$, would be calculated as,

$$f_{i-1,i} = \int_{b}^{a} V(x)dy \qquad 3.1$$

where the line between grid points *a* and *b* is the border between cells *i*-1 and *i* (Figure 3-1). Similarly, for flow in the y-direction with velocity, V(y), defined at each grid point (a, d) the flow, $f_{i-N,i}$, is given by,

$$f_{i-N,i} = \int_a^d V(y)dx \qquad 3.2$$

where N is the total number of cells formed by the grid.

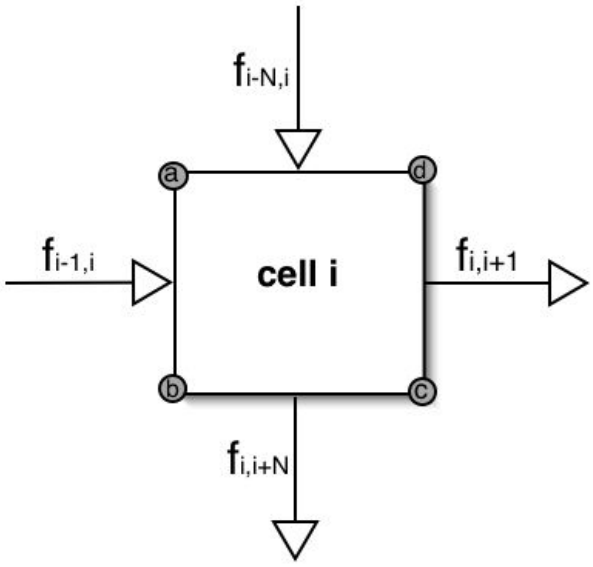

Figure 3-1. Flows into and out of cell *i* are determined by integrating along the borders with each neighboring cells (*i*-1, *i*+1, *i*-N, and *i*+N). Velocity at each of the four grid points (a, b, c, and d) is defined, so that f_{ij} represents an average flow between any two grid points.

3.1.1 Example 1: Flow between two parallel boundaries with a linear velocity profile

This simple example of a linear velocity profile, like the four-compartment networks described in Chapter 1, has the added benefit of offering the reader the opportunity to perform the required calculations rather quickly by hand. Steady state, laminar flow between two flat, parallel boundaries can be achieved by accelerating the

bottom boundary to a velocity, V_0, and holding the top boundary fixed, so that V(y=0) = 0 and V(y=R) = V_0 (Figure 3-2). Both boundaries are of length, L, and separated by a distance of R such that L >> R and end effects are negligible.

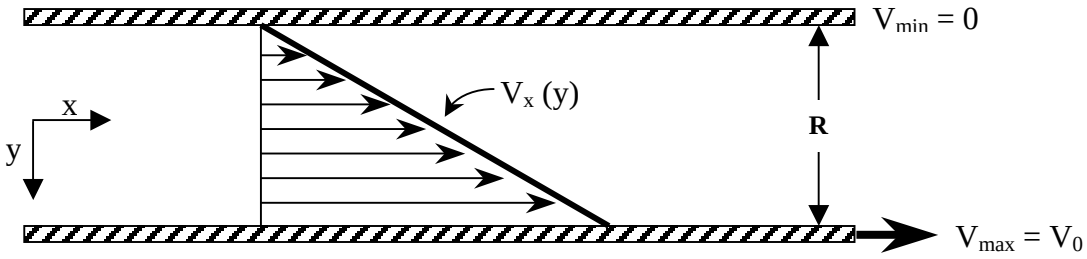

Figure 3-2. Steady state laminar velocity profile for fluid flow between two parallel boundaries.

Once the fluid reaches a steady state velocity, a linear velocity profile between the two boundaries is given by,

$$V_x = \frac{V_0}{R}(y - R) + V_0 \qquad 3.3$$

where y = 0 at the top boundary and y = R at the bottom boundary. Overlaying the flow field with a grid of N x N cells and then translating from an x-y coordinate system to an i-j coordinate system results in a new equation for the velocity with V_x defined at every grid point, V(i, j),

$$V_x = \frac{V_0}{N}(i - N) + V_0 \qquad 3.4$$

where *i* is incremented from 0 to N. The velocity varies only in the vertical direction, so all flows, f_{ij}, in this flow field are found by calculating a line integral between each pair of grid points in the vertical direction. The average flow between any two grid points, *i* and *i+1*, is calculated as,

$$f_{ij} = \int_{i}^{i+1} V_x dy = \frac{V_0}{2N}(2i+1) \qquad 3.5$$

and again to cover the entire flow field *i* is incremented from 0 to N. Each flow, f_{ij}, is stored in a N^2 x N^2 flow matrix in preparation for calculating the information indices.

3.1.1.1 Appling network analysis to flow with a linear velocity profile

Network indices characterizing the flow are calculated by applying the equations introduced in Chapter 1 to the flows calculated from (3.5) and stored in the flow matrix. As in the cellular automata examples of Chapter 2, wrap around boundary conditions are utilized to allow continuous flow in the horizontal direction. For N = 10 and V_0 = 3 cm s^{-1} the flow velocities (Table 5) increase linearly from *i* = 0 to *i*= N, with a maximum velocity, V_0 = 3 cm s^{-1}, occurring at *i* = N.

Table 5. Velocity values for the linear flow profile with N = 10 and V_0 = 3 cm s^{-1}. Velocities are in cm s^{-1} and vary only with *i*.

i \ *j*	0	1	2	3	4	5	6	7	8	9	10
0	0	0	0	0	0	0	0	0	0	0	0
1	0.30	0.30	0.30	0.30	0.30	0.30	0.30	0.30	0.30	0.30	0.30
2	0.60	0.60	0.60	0.60	0.60	0.60	0.60	0.60	0.60	0.60	0.60
3	0.90	0.90	0.90	0.90	0.90	0.90	0.90	0.90	0.90	0.90	0.90
4	1.20	1.20	1.20	1.20	1.20	1.20	1.20	1.20	1.20	1.20	1.20
5	1.50	1.50	1.50	1.50	1.50	1.50	1.50	1.50	1.50	1.50	1.50
6	1.80	1.80	1.80	1.80	1.80	1.80	1.80	1.80	1.80	1.80	1.80
7	2.10	2.10	2.10	2.10	2.10	2.10	2.10	2.10	2.10	2.10	2.10
8	2.40	2.40	2.40	2.40	2.40	2.40	2.40	2.40	2.40	2.40	2.40
9	2.70	2.70	2.70	2.70	2.70	2.70	2.70	2.70	2.70	2.70	2.70
10	3.00	3.00	3.00	3.00	3.00	3.00	3.00	3.00	3.00	3.00	3.00

The flows are stored in a 100 x 100 flow matrix, which is too large to present in the text in its entirety. However, for laminar flow most entries into the flow matrix equal zero, so it is possible to present all nonzero flows (Table 6). Like the velocities, the flows only vary with *i*, and are maximum at *i* = N. Since each flow is calculated along a line joining two grid points, only ten flows are calculated for the 11 grid point velocities presented (Table 5).

Table 6. Flows calculated by the model for the linear flow profile with N = 10 and V_0 = 3 cm s^{-1}. Flows are calculated along the line joining grid points *i* and *i* + 1 and vary only with *i*. Values have units of cm^3 s^{-1}.

i/i+1 \ *j*	0	1	2	3	4	5	6	7	8	9	10
0/1	0.15	0.15	0.15	0.15	0.15	0.15	0.15	0.15	0.15	0.15	0.15
1/2	0.45	0.45	0.45	0.45	0.45	0.45	0.45	0.45	0.45	0.45	0.45
2/3	0.75	0.75	0.75	0.75	0.75	0.75	0.75	0.75	0.75	0.75	0.75
3/4	1.05	1.05	1.05	1.05	1.05	1.05	1.05	1.05	1.05	1.05	1.05
4/5	1.35	1.35	1.35	1.35	1.35	1.35	1.35	1.35	1.35	1.35	1.35
5/6	1.65	1.65	1.65	1.65	1.65	1.65	1.65	1.65	1.65	1.65	1.65
6/7	1.95	1.95	1.95	1.95	1.95	1.95	1.95	1.95	1.95	1.95	1.95
7/8	2.25	2.25	2.25	2.25	2.25	2.25	2.25	2.25	2.25	2.25	2.25
8/9	2.55	2.55	2.55	2.55	2.55	2.55	2.55	2.55	2.55	2.55	2.55
9/10	2.85	2.85	2.85	2.85	2.85	2.85	2.85	2.85	2.85	2.85	2.85

The total system throughput, f.., is equal to 165 cm^3 s^{-1}, and is representative of a measure of mass transport or flux. This is easily verified by summing all nonzero flows (Table 6). Organization or the ordered component of the flow is measured by the AMI, which is equal to 6.508 bits of information. The overall network ascendency, A, for this flow field is calculated as A = (AMI) x (f..) = 1,074 flow bits. Identifying which flows within the flow field have the greatest contribution to the A is accomplished by plotting the distribution of the A (Figure 3-3). As one might expect, the flows with the greatest contribution to the A are located at the bottom of the flow field where the velocity is greatest. A similar plot of the distribution of the sensitivities of the A to individual flows highlights those flows that exhibit the greatest resistance to the overall flow or activity within the flow field (Figure 3-4). Areas with the highest sensitivity values are effectively acting as bottlenecks in a flow field. In a more complex flow field with

multidirectional flows, the locations of bottlenecks within the flow field may not be as intuitively obvious.

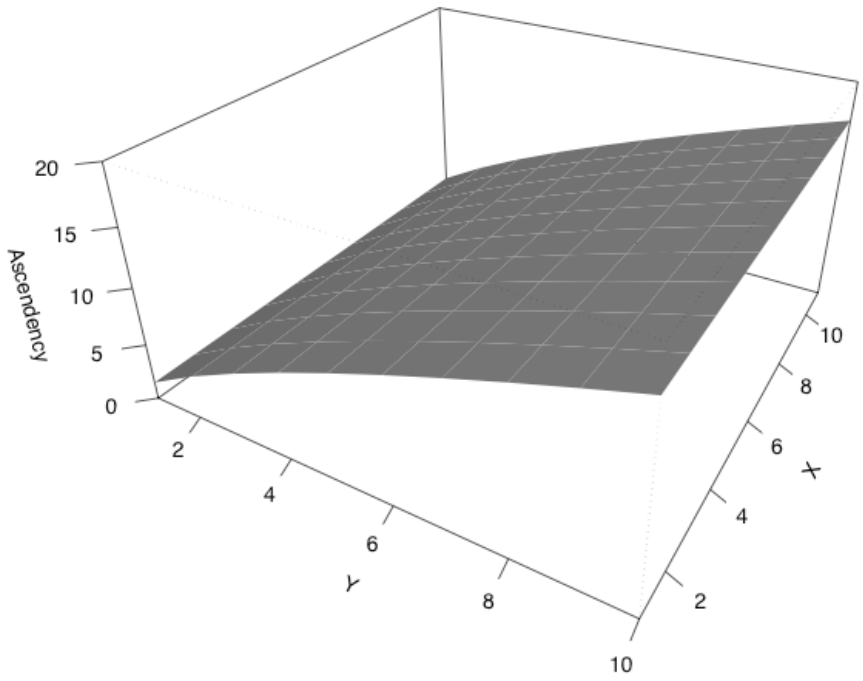

Figure 3-3. 3D contour plot of the contribution of each flow, f_{ij}, in the linear flow field to the overall network ascendency, A. Flow is in the x-direction and flow velocity, V_x, is such that $V_x = 0$ at y = 0, and $V_x = V_0 = 3$ cm s^{-1} at y = 10.

Even though the velocity profile varies linearly in the x-direction, both the A profile and the sensitivity of the A profile vary as a function of $\log_2$ in the x-direction, by definition. This dependency is more pronounced in the sensitivities (Figure 3-4), which are not scaled by the flows, and explains how areas of low activity and high resistance are highlighted in the calculation of the sensitivity of the A to each flow.

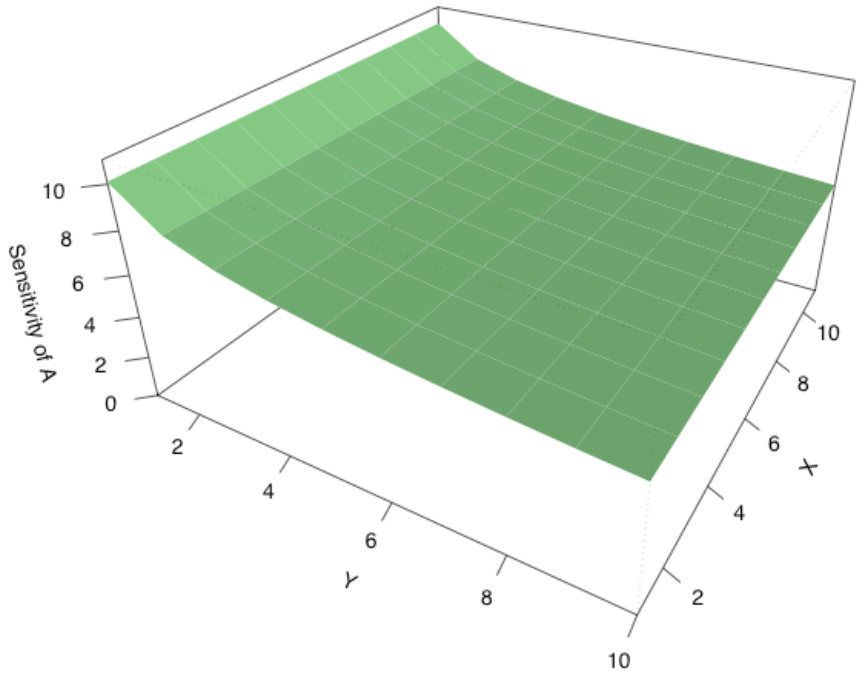

Figure 3-4. Sensitivities of the overall ascendency to individual flows in the linear flow field. Flow is in the x-direction and flow velocity, V_x, is such that $V_x = 0$ at y = 0, and $V_x = V_0 = 3$ cm s^{-1} at y = 10.

3.1.2 Example 2: Flow between two parallel boundaries with a parabolic velocity profile

A flow field with a parabolic velocity profile symmetric about the centerline between two parallel boundaries has V_{max} occurring along the centerline and $V_{min} = 0$ at both boundaries (Figure 3-5). As in the previous example, the length of the boundaries, L, is much greater than R to avoid end effects.

After a steady state flow is reached, the velocity profile is described by,

$$V_x = K\left[1 - \frac{(2y - R)^2}{R^2}\right] \qquad 3.6$$

where $V_x = 0$ at $y = 0$ and $y = R$, and $V_x = K = V_{max}$ at $y = R/2$. The constant K is defined as,

$$K \equiv \frac{\Delta P R^2}{4\mu L} \qquad 3.7$$

where ΔP represents a pressure gradient in the direction of the flow and μ is the viscosity of the fluid.

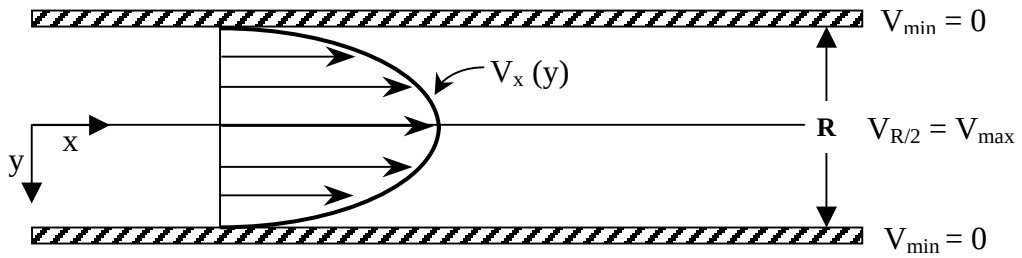

Figure 3-5. Steady state laminar parabolic velocity profile for fluid flow between two parallel boundaries.

Values for the constants were chosen to make a direct comparison between the results from each of the four examples as simple and straightforward as possible. A maximum velocity of 3 cm s^{-1} was chosen as representative of oceanic currents. The separation between boundaries, R, was set at 10 m, and the length of the boundaries, L,

was set at 1 km. The viscosity, μ, of water at 20 °C is 0.001 kg m^{-1} s^{-1}, so for K equal to 3 cm s^{-1}, $\Delta P = 1.2 \times 10^{-3}$ N m^{-2}.

The values for the constants are set with the understanding that laminar flow is maintained if the Reynolds Number (Re) is less than about 2,500 (Mann and Lazier 1996). For the values chosen,

$$\mathrm{Re} = \frac{\rho V_x R}{\mu} = 3.0x10^5 >> 2{,}500 \qquad 3.8$$

where ρ = 1,000 kg m^{-3} is the density of water. Clearly, laminar flow cannot be assumed for the conditions described above. If constants are chosen so that Re < 2,500, then the flow values, f_{ij}, are invariably small, and the information indices also calculate to be quite small. Comparing organization among different flow fields using the differences between small numbers is a bit cumbersome and detracts from the focus of the research, which is to demonstrate the applicability of network analysis to fluid flow, and not to model the physical behavior of actual fluids.

The velocity equation (3.6) is translated from the x-y coordinate system to the i-j coordinate system,

$$V_x = K\left[1 - \frac{(2i - N)^2}{N^2}\right] \qquad 3.9$$

where *i* is incremented from 0 to N. The velocity varies only in the vertical direction, so all flows, f_{ij}, in this flow field are found by calculating a line integral between each pair of grid points in the vertical direction. The average flow between any pair of grid points, *i* and *i+1*, is calculated as,

$$f_{ij} = \frac{2K}{3N^2}\left[-6i^2 - 6i(1-N) + 3N - 2\right] \qquad 3.10$$

by integrating (3.9) from *i* to *i+1*.

3.1.2.1 Appling network analysis to flow with a parabolic velocity profile

Wrap around boundary conditions apply in the x-direction so that flow is continuous in that direction. The velocity matrix (Table 7) shows that velocity increases from $V_x = 0$ at $i = 0$ to a maximum velocity at the center of the flow field where $V_x = K = 3$ cm s^{-1}. The velocity then decreases symmetrically to equal 0 at $i = N$.

Table 7. Velocity values for the parabolic flow profile where N = 10 and V_0 = 3 cm s^{-1}. Velocities are in cm s^{-1} and vary only with *i*.

i \ *j*	0	1	2	3	4	5	6	7	8	9	10
0	0.00	0.00	0.00	0.00	0.00	0.00	0.00	0.00	0.00	0.00	0.00
1	1.08	1.08	1.08	1.08	1.08	1.08	1.08	1.08	1.08	1.08	1.08
2	1.92	1.92	1.92	1.92	1.92	1.92	1.92	1.92	1.92	1.92	1.92
3	2.52	2.52	2.52	2.52	2.52	2.52	2.52	2.52	2.52	2.52	2.52
4	2.88	2.88	2.88	2.88	2.88	2.88	2.88	2.88	2.88	2.88	2.88
5	3.00	3.00	3.00	3.00	3.00	3.00	3.00	3.00	3.00	3.00	3.00
6	2.88	2.88	2.88	2.88	2.88	2.88	2.88	2.88	2.88	2.88	2.88
7	2.52	2.52	2.52	2.52	2.52	2.52	2.52	2.52	2.52	2.52	2.52
8	1.92	1.92	1.92	1.92	1.92	1.92	1.92	1.92	1.92	1.92	1.92
9	1.08	1.08	1.08	1.08	1.08	1.08	1.08	1.08	1.08	1.08	1.08
10	0.00	0.00	0.00	0.00	0.00	0.00	0.00	0.00	0.00	0.00	0.00

Examining all nonzero flows from the 100 x 100 flow matrix (Table 8) shows that, as anticipated, the flows between vertically spaced grid points are greatest in the center of the flow field and minimal at the boundaries.

Table 8. Flows calculated along the line joining grid points *i* and *i* + 1 for a fluid with a parabolic velocity profile where N = 10 and V_0 = 3 cm s^{-1}. Flows vary only with *i*. Values are in units of cm^3 s^{-1}.

i/i+1 \ *j*	0	1	2	3	4	5	6	7	8	9	10
0/1	0.56	0.56	0.56	0.56	0.56	0.56	0.56	0.56	0.56	0.56	0.56
1/2	1.52	1.52	1.52	1.52	1.52	1.52	1.52	1.52	1.52	1.52	1.52
2/3	2.24	2.24	2.24	2.24	2.24	2.24	2.24	2.24	2.24	2.24	2.24
3/4	2.72	2.72	2.72	2.72	2.72	2.72	2.72	2.72	2.72	2.72	2.72
4/5	2.96	2.96	2.96	2.96	2.96	2.96	2.96	2.96	2.96	2.96	2.96
5/6	2.96	2.96	2.96	2.96	2.96	2.96	2.96	2.96	2.96	2.96	2.96
6/7	2.72	2.72	2.72	2.72	2.72	2.72	2.72	2.72	2.72	2.72	2.72
7/8	2.24	2.24	2.24	2.24	2.24	2.24	2.24	2.24	2.24	2.24	2.24
8/9	1.52	1.52	1.52	1.52	1.52	1.52	1.52	1.52	1.52	1.52	1.52
9/10	0.56	0.56	0.56	0.56	0.56	0.56	0.56	0.56	0.56	0.56	0.56

The total system throughput, f.., for flow with a parabolic velocity profile is 220 cm^3 s^{-1}. This calculation is easily verified by summing all nonzero flows (Table 8). The ordered component of the flow is measured by the AMI, which is equal to 6.620 bits of information. The network ascendency, A, for a parabolic flow profile is calculated as A = (AMI) x (f..) = 1,456 flow bits. Identifying the contribution of each individual flow in the flow field to the A is accomplished visually by plotting the distribution of the A over the flow field (Figure 3-6). As one might expect from the velocity profile, the flows with the greatest contribution to the A are located in the center of the flow field where the velocity is greatest. Fluid moves more rapidly through the cells overlaying the center of the flow field, so the flows through those same cells are greater than at any other location in the flow field.

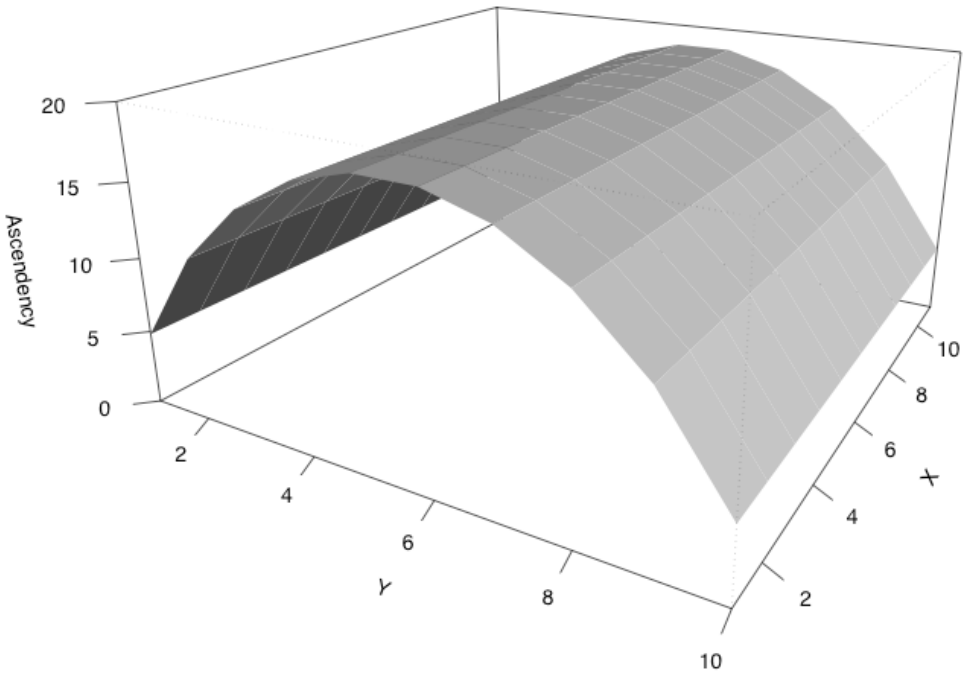

Figure 3-6. 3D contour plot of the contribution of each flow, f_{ij}, in the parabolic flow field to the overall network ascendency, A. Flow is in the x-direction and flow velocity, V_x, is such that $V_x = 0$ at y = 0 and y = 10, and $V_x = V_0 = 3$ cm s^{-1} at y = 5.

A similar plot of the distribution of the sensitivity of the A to individual flows highlights those flows that exhibit the greatest resistance to the overall flow or activity within the flow field (Figure 3-7). Areas with the highest sensitivity values may be regarded as bottlenecks to the flow. These areas exhibit the fewest number of flows, a characteristic that might also be attributable to calm waters on the downstream side of an obstruction to flow in a river, for example. In a more complex flow field where the dominant flow is redirected multiple times or must circumvent multiple obstructions, the locations of bottlenecks within the flow field may not be obvious in the distribution of the ascendency, because the ascendency is scaled by each flow, f_{ij}.

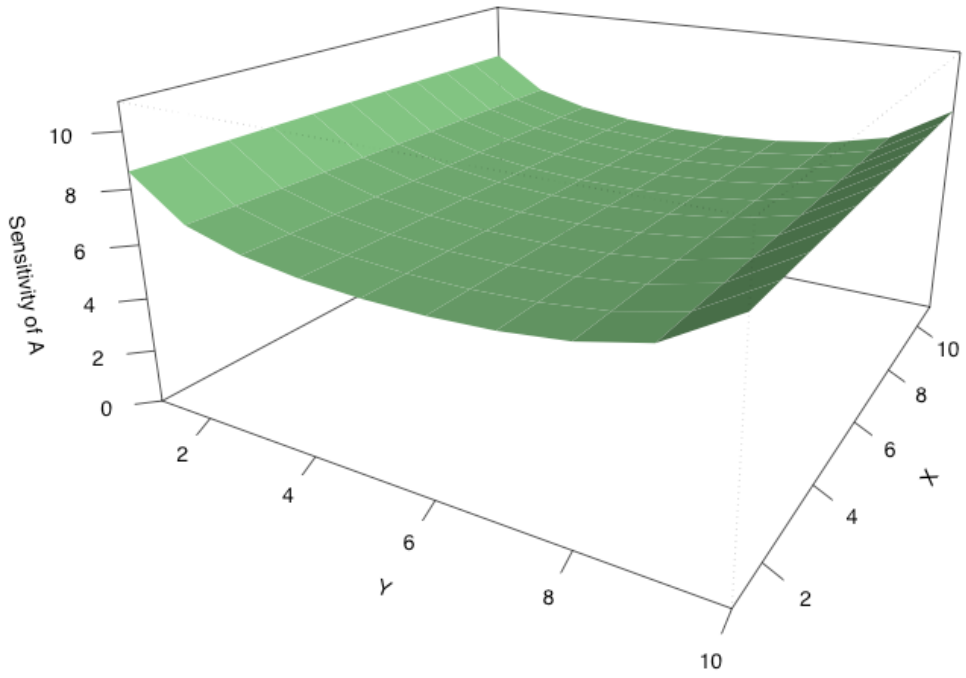

Figure 3-7. Sensitivities of the overall ascendency to individual flows in the parabolic flow field. Flow is in the x-direction and flow velocity, V_x, is such that $V_x = 0$ at y = 0 and y = 10, and $V_x = V_0 = 3$ cm s^{-1} at y = 5.

The sensitivities, on the other hand, are not scaled by the flows, and vary on a log scale, which tends to amplify smaller values. In the parabolic flow field, it is only the flows adjacent to the boundaries that are obviously highlighted (Figure 3-7); the sensitivities associated with the remainder of the flows are not easily distinguishable from the maximum central flow, which stands in contrast to the ascendency and velocity profiles. Shear stress in the fluid is greatest near the boundaries, where frictional forces between the fluid and the boundaries cause resistance to the flow. The relative magnitude and location of greatest resistance is quantified by the sensitivity values.

3.1.3 Example 3: Adjacent flow of two immiscible fluids with an asymmetric velocity profile

A flow field consisting of two immiscible fluids, $Fluid_1$ and $Fluid_2$, with viscosities μ_1 and μ_2 (where $\mu_2 > \mu_1$), and enclosed on two sides by parallel boundaries has an asymmetric velocity profile with V_{max} occurring in the fluid with the lower viscosity (i.e. $Fluid_1$) (Figure 3-8). If the entire flow field is subject to the same pressure gradient force, then the velocity, V_x, at both boundaries will be zero, just as in the pervious example with a parabolic velocity profile; however, both fluids do not reach the same steady state velocities away from the boundaries because of their differing viscosities.

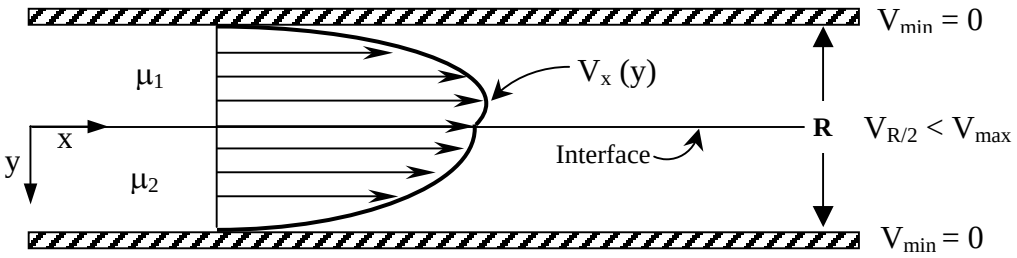

Figure 3-8. Steady state laminar velocity profile for two immiscible fluids of differing viscosities between two parallel boundaries and subject to a pressure gradient inducing flow in the x-direction.

$Fluid_2$ has a greater resistance to flow than $Fluid_1$, and requires a greater pressure gradient to achieve a matching velocity profile. The same pressure gradient generates flow in both fluids, so $Fluid_2$ will lag behind $Fluid_1$. The maximum velocity should no longer be at the centerline, as it was in the previous example. To maintain continuity of flow across

the interface, the velocity of both fluids must be the same at the interface. One could imagine the more viscous $Fluid_2$ effectively dragging on the adjacent portion of $Fluid_1$ at the interface and reducing its velocity. The maximum velocity is achieved within the domain of $Fluid_1$ just off the centerline at the point where the shear induced by the influence of $Fluid_2$ and the shear induced by friction at the boundary are both zero (Bird et al. 1960). In the model for this example, the velocity profiles are expressed as one half of different parabolic functions, where the curvature of the profile for $Fluid_2$ is flatter than the profile for $Fluid_1$, but both profiles reach the same velocity at the interface.

After steady state flow is achieved, the velocities, V_x^I and V_x^{II}, are given by,

$$V_x^I = -K_1(2y-R)^2 - \frac{C_1^I}{\mu_1}(2y-R)^2 + C_2^I \qquad 3.12a$$

$$V_x^{II} = -K_2(2y-R)^2 - \frac{C_1^{II}}{\mu_2}(2y-R)^2 + C_2^{II} \qquad 3.12b$$

where the K_1 and K_2 are defined as,

$$K_1 = \frac{\Delta P}{2\mu_1 L} \qquad 3.13a$$

$$K_2 = \frac{\Delta P}{2\mu_2 L} \qquad 3.13b$$

and the constants C_1 and C_2 are calculated by applying the following three boundary conditions:

$$\underline{BC\#1}:\quad at\quad y=\frac{R}{2}\qquad V_x^I=V_x^{II}\qquad \therefore\quad C_2^I=C_2^{II}=C_2$$

$$\underline{BC\#2}:\quad at\quad y=0\qquad V_x^I=0=-K_1R^2+\frac{C_1^I}{\mu_1}R+C_2\qquad \therefore\quad C_2=K_1R^2-\frac{C_1^I}{\mu_1}R$$

$$\underline{BC\#3}:\quad at\quad y=R\qquad V_x^{II}=0=-K_2R^2+\frac{C_1^{II}}{\mu_{II}}R+C_2$$
$$=-K_2R^2+\frac{C_1^{II}}{\mu_{II}}R+\left(K_1R^2-\frac{C_1^I}{\mu_1}R\right)$$

The momentum transport across the interface must be continuous (Bird et al. 1960), therefore $C_1^{I} = C_1^{II} = C_1$, and the boundary conditions may now be used to solve for C_1 and C_2,

$$C_1=\frac{R(K_1-K_2)}{\left(\frac{1}{\mu_1}+\frac{1}{\mu_2}\right)}\qquad C_2=K_1R^2-\frac{R^2(K_1-K_2)}{\mu_1\left(\frac{1}{\mu_1}+\frac{1}{\mu_2}\right)} \qquad 3.14$$

Values for the constants were chosen to make a direct comparison between the results from each of the four examples as simple and straightforward as possible. A maximum velocity of 3 cm s^{-1} was chosen as representative of oceanic currents. The separation between boundaries, R, was set at 10 m, and the length of the boundaries, L, was set at 1 km. Choosing water as the less viscous $Fluid_1$, μ_1 = 0.001 kg m^{-1} s^{-1} at 20 °C, and choosing seawater as $Fluid_2$, μ_2 = 0.0012 kg m^{-1} s^{-1} at 20 °C (Elert 2002). For the same pressure gradient used in the previous example, $\Delta P = 1.2 \times 10^{-3}$ N m^{-2}, a maximum velocity of ~2.7 cm s^{-1} is reached in $Fluid_1$, because of the influence of more viscous

$Fluid_2$. Other fluids with higher viscosities (e.g. Olive Oil, $\mu = 0.084$ kg m^{-1} s^{-1}) were tested, but the variation in the flow profile between fluids was so exaggerated that any characterization of the flow field by the information indices would have been dominated by the obvious disparity in the velocities of the fluids.

As in the previous example, the length of the boundaries, L, is much greater than R to avoid end effects, and laminar flow is assumed even though results of the Reynolds number calculations for both fluids contradict that assumption. The Reynolds number for water is about the same as in the previous example, 2.7×10^5, and the Reynolds number for seawater is somewhat less at 2.3×10^5 ($\rho \sim 1030$ kg m^{-3}), but still well beyond the threshold for purely laminar flow (Mann and Lazier 1996).

The velocity equations (3.12a and 3.12b) are translated from the x-y coordinate system to the i-j coordinate system,

$$V_x^I = -K_1(2i - N)^2 - \frac{C_1}{\mu_1}(2i - N)^2 + C_2 \qquad 3.15a$$

$$V_x^{II} = -K_2(2i - N)^2 - \frac{C_1}{\mu_2}(2i - N)^2 + C_2 \qquad 3.15b$$

by a direct exchange of *y* for *i* and R for N. The same substitution of variables is made for C_1 and C_2 in (3.14). At the interface between $Fluid_1$ and $Fluid_2$ (i.e. at $i = 5$) $V_x^{I} = V_x^{II} = C_2$. The velocity varies only in the vertical direction, so all flows, f_{ij}, in this flow field are found by calculating the line integral of (3.15a and 3.15b) between each pair of grid

points in the vertical direction. The average flow between any pair of grid points, *i* and *i*+1, is calculated as,

$$f_{ij}^{I,II} = -\frac{K_{1,2}}{3}\left(12i^2 + 12i + 4 - 12Ni - 6N + 3N^2\right) - \frac{C_1}{\mu_{1,2}}\left(2i + 1 - N\right) + C_2 \qquad 3.16$$

where f_{ij}^{I} is calculated using K_1 and μ_1 and represents the flows in $Fluid_1$, and f_{ij}^{II} is calculated using K_2 and μ_2 and represents the flows in $Fluid_2$.

3.1.3.1 Appling network analysis to flow of two adjacent immiscible fluids between two parallel boundaries

Wrap around boundary conditions are applied so that flow is continuous in the x-direction. Velocity increases from $V_x = 0$ at $i = 0$ to a maximum, $V_x = 2.7$ cm s^{-1}, at the interface where $i = 5$ (Table 9). The velocity then decreases asymmetrically to equal 0 at $i = N$. Velocity values in the domain of $Fluid_1$ are all greater than their corresponding pairs in the domain of $Fluid_2$.

Table 9. Velocity values for flow of two adjacent immiscible fluids where with N = 10 and V_{max} = 3 cm s^{-1} at *i* = 5. Velocities are in cm s^{-1} and vary only with *i*.

i \ *j*	0	1	2	3	4	5	6	7	8	9	10
0	0.00	0.00	0.00	0.00	0.00	0.00	0.00	0.00	0.00	0.00	0.00
1	1.03	1.03	1.03	1.03	1.03	1.03	1.03	1.03	1.03	1.03	1.03
2	1.81	1.81	1.81	1.81	1.81	1.81	1.81	1.81	1.81	1.81	1.81
3	2.36	2.36	2.36	2.36	2.36	2.36	2.36	2.36	2.36	2.36	2.36
4	2.66	2.66	2.66	2.66	2.66	2.66	2.66	2.66	2.66	2.66	2.66
5	2.73	2.73	2.73	2.73	2.73	2.73	2.73	2.73	2.73	2.73	2.73
6	2.58	2.58	2.58	2.58	2.58	2.58	2.58	2.58	2.58	2.58	2.58
7	2.24	2.24	2.24	2.24	2.24	2.24	2.24	2.24	2.24	2.24	2.24
8	1.69	1.69	1.69	1.69	1.69	1.69	1.69	1.69	1.69	1.69	1.69
9	0.95	0.95	0.95	0.95	0.95	0.95	0.95	0.95	0.95	0.95	0.95
10	0.00	0.00	0.00	0.00	0.00	0.00	0.00	0.00	0.00	0.00	0.00

The distribution of all nonzero flows from the 100 x 100 flow matrix (Table 10) shows that the flows are greatest in the domain of $Fluid_1$ and decrease at slightly steeper gradient in the domain of $Fluid_2$. In the matrix, the interface occurs between rows 4/5 and 5/6 (Table 10).

Table 10. Flows calculated along the line joining grid points *i* and *i* + 1 for two adjacent immiscible fluids where N = 10 and V_{max} = 3 cm s^{-1}. Values are in units of cm^3 s^{-1}.

i/i+1 *j*	0	1	2	3	4	5	6	7	8	9	10
0/1	0.53	0.53	0.53	0.53	0.53	0.53	0.53	0.53	0.53	0.53	0.53
1/2	1.44	1.44	1.44	1.44	1.44	1.44	1.44	1.44	1.44	1.44	1.44
2/3	2.10	2.10	2.10	2.10	2.10	2.10	2.10	2.10	2.10	2.10	2.10
3/4	2.53	2.53	2.53	2.53	2.53	2.53	2.53	2.53	2.53	2.53	2.53
4/5	2.71	2.71	2.71	2.71	2.71	2.71	2.71	2.71	2.71	2.71	2.71
5/6	2.73	2.73	2.73	2.73	2.73	2.73	2.73	2.73	2.73	2.73	2.73
6/7	2.43	2.43	2.43	2.43	2.43	2.43	2.43	2.43	2.43	2.43	2.43
7/8	1.98	1.98	1.98	1.98	1.98	1.98	1.98	1.98	1.98	1.98	1.98
8/9	1.33	1.33	1.33	1.33	1.33	1.33	1.33	1.33	1.33	1.33	1.33
9/10	0.49	0.49	0.49	0.49	0.49	0.49	0.49	0.49	0.49	0.49	0.49

The total system throughput, f.., for the flow of two adjacent immiscible fluids is 201 cm^3 s^{-1}. This calculation is easily verified by summing all nonzero flows (Table 10). The ordered component of the flow is measured by the AMI, which is equal to 6.618 bits of information. The network ascendency, A, a combination of the activity and organization of the flow field, is calculated as A = (AMI) x (f..) and A = 1,330 flow bits. Displaying the contribution of each individual flow in the flow field to the A is accomplished by plotting the distribution of the A over the flow field (Figure 3-9). As one might expect from the matrix of flows, the greatest contribution to the A is from the region within the domain of $Fluid_1$ where the velocities are greater. $Fluid_1$ moves more rapidly through the flow field, so the flows within the domain of $Fluid_1$ are greater than the flows within the domain of $Fluid_2$, and those same regions have the greatest contributions to the A.

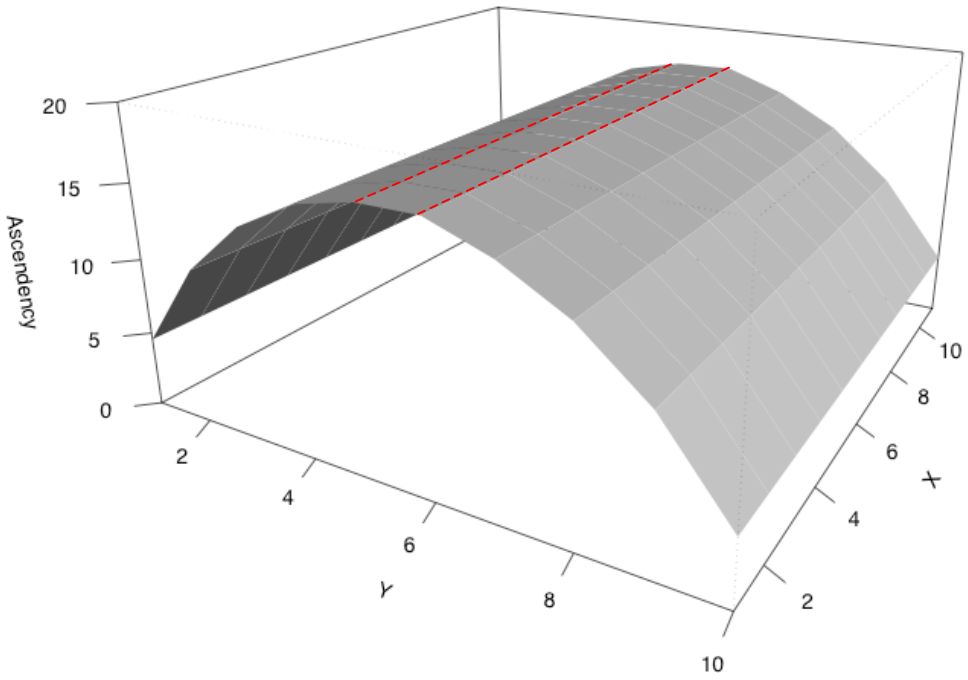

Figure 3-9. 3D contour plot of the contribution of each flow, f_{ij}, of two adjacent immiscible fluids to the overall flow field ascendency. Flow is in the x-direction and flow velocity, V_x, is such that $V_x = 0$ at y = 0 and y = 10, and V_x is maximum at y = 5. Contributions to the ascendency mirror the velocity profile. The red dashed lines indicate the location of the flows between y = 4 and the interface and the interface and y = 6.

A similar plot of the distribution of the sensitivity of the A to individual flows highlights those flows that exhibit the greatest resistance within the flow field, or exhibit the lowest activity within the flow field (Figure 3-10). Areas with the highest sensitivity values may be regarded as bottlenecks to the overall flow, because they exhibit the least amount of ordered activity within the flow field. Activity, measured by the amount of medium transferred, is lowest within the domain of $Fluid_2$, and correspondingly the highest sensitivity values are found in the domain of $Fluid_2$ where the resistance is highest (Figure 3-10).

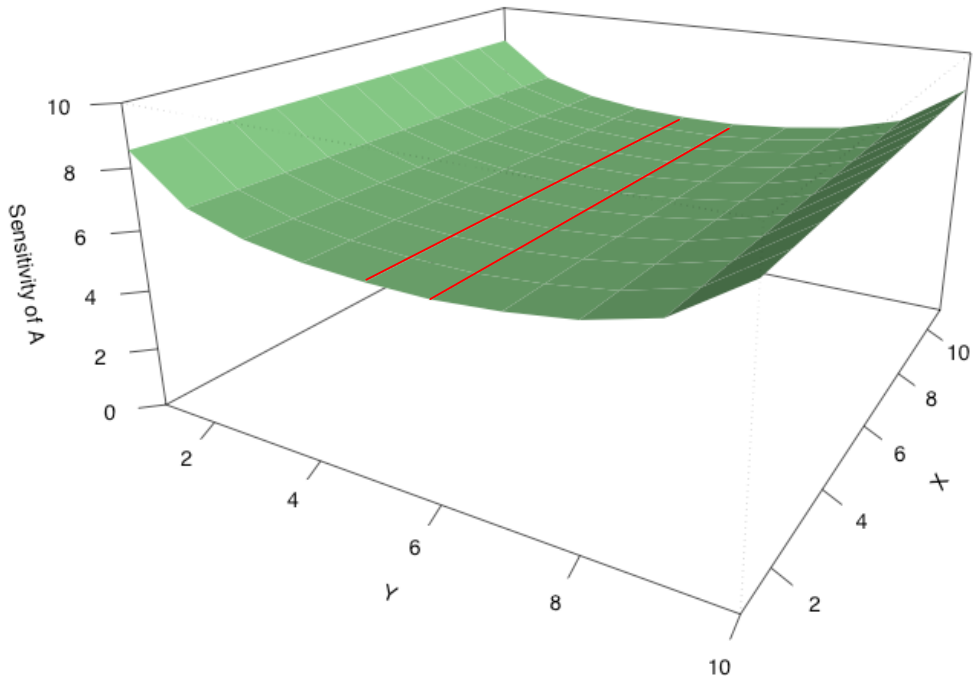

Figure 3-10. Sensitivity of the ascendency to individual flows in a flow field with two adjacent immiscible fluids ($Fluid_1$ and $Fluid_2$). Flow is in the x-direction and flow velocity, V_x, is such that $V_x = 0$ at y = 0 and y = 10, and V_x is maximum between y = 2 and y = 3. The lower viscosity fluid ($Fluid_1$) occupies the region between y = 1 and y = 5, and $Fluid_2$ occupies the region between y = 6 and y = 10. Sensitivity values are indicative of regions of low activity in the flow field (e.g. bottlenecks). The red dashed lines indicate the location of the flows between y = 4 and the interface and the interface and y = 6.

The dynamics of the flow field, as measured by the ascendency, is most sensitive to changes in the smallest flows. Adjustments in the largest flows will certainly affect the ascendency of the flow field, but changes to the smallest flows (i.e. flows with the highest sensitivities) will have a greater impact on the ascendency.

3.1.4 Example 4: Circular flow

An incompressible fluid enclosed by a circular boundary (e.g. a cylinder), which is rotating at a constant velocity, V_o, has a laminar velocity profile described by,

$$V = V_\theta + V_r = \frac{r}{R} V_0 \qquad 3.18$$

where V_θ is the tangential velocity calculated at each grid point along a radius of length R (Figure 3-11). For steady state laminar flow the radial velocity, V_r, is equal to zero (the axial velocity, V_z, is also equal to zero under these conditions). The velocity varies from zero at the center to V_o at the boundary, and is calculated from (3.18) at 10 equally spaced grid points along 11 radii separated by about 32.7° around the circle, for a total of 110 grid points at which the velocity is defined analytically.

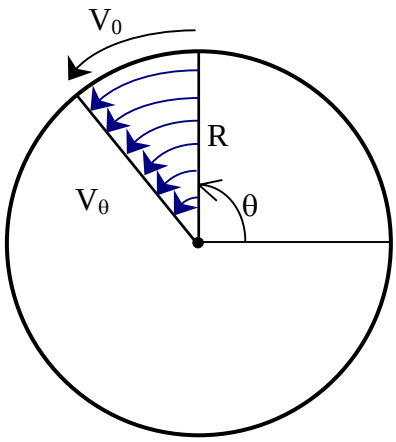

Figure 3-11. Schematic diagram of the velocity profile for steady state laminar flow of an incomopressible fluid induced by an outer boundary rotating at a constant velocity, V_0. The circle formed is of radius R, and the velocity at any point within the flow field, V_θ, is a function of R.

Of the four examples described in this chapter, this is the only one that has true two-dimensional flow; although, the calculations are simplified considerably by working in cylindrical coordinates instead of the Cartesian coordinates used in the other three examples. Since the velocity at each fraction of R (i.e. r/R) is constant around the entire flow field, converting (3.18) from cylindrical coordinates into i-j space simply requires swapping *i* for r and N for R,

$$V_\theta = \frac{i}{N} V_0 \qquad 3.19$$

where N is the total number and *i* increments from zero to N. Integrating (3.19) along each line segment connecting grid points *i* and *i* + 1 with respect to *i* results in an expression describing the flow, f_{ij}, between each cell,

$$f_{ij} = \int_{i}^{i+1} \frac{iV_\theta}{N} di = \frac{V_\theta}{2N}(2i+1) \qquad 3.20$$

3.1.4.1 Appling network analysis to laminar circular flow

From the velocity matrix (Table 11) one can see that the velocity increases radially from zero at the center to a maximum of 3 cm s^{-1} at the boundary. The velocities along concentric circles a distance *i*/R from the center are equal. In actuality, the velocities along each concentric circle represent an average of the linear velocity profile between concentric bands that must exist in order for flow to be continuous along R.

Table 11. Velocity values for circular flow with N = 10 and V_0 = 3 cm s^{-1}. Velocities are in cm s^{-1} and vary only along the radius represented by the index *i*.

i \ ***j***	0	1	2	3	4	5	6	7	8	9	10
0	0	0	0	0	0	0	0	0	0	0	0
1	0.30	0.30	0.30	0.30	0.30	0.30	0.30	0.30	0.30	0.30	0.30
2	0.60	0.60	0.60	0.60	0.60	0.60	0.60	0.60	0.60	0.60	0.60
3	0.90	0.90	0.90	0.90	0.90	0.90	0.90	0.90	0.90	0.90	0.90
4	1.20	1.20	1.20	1.20	1.20	1.20	1.20	1.20	1.20	1.20	1.20
5	1.50	1.50	1.50	1.50	1.50	1.50	1.50	1.50	1.50	1.50	1.50
6	1.80	1.80	1.80	1.80	1.80	1.80	1.80	1.80	1.80	1.80	1.80
7	2.10	2.10	2.10	2.10	2.10	2.10	2.10	2.10	2.10	2.10	2.10
8	2.40	2.40	2.40	2.40	2.40	2.40	2.40	2.40	2.40	2.40	2.40
9	2.70	2.70	2.70	2.70	2.70	2.70	2.70	2.70	2.70	2.70	2.70
10	3.00	3.00	3.00	3.00	3.00	3.00	3.00	3.00	3.00	3.00	3.00

For laminar flow most entries into the flow matrix equal zero. Examining all nonzero flows (Table 12) reveals that, like the velocities, the flows vary only with *i*, and are maximum at *i* = N along the circular boundary. Each flow is calculated along a line joining two grid points, so only ten flows are calculated between the 11 grid point velocities (Table 11). A three-dimensional contour plot of the flows with velocity increasing in the positive z-directions shows that the flows increase radially in all directions (Figure 3-12).

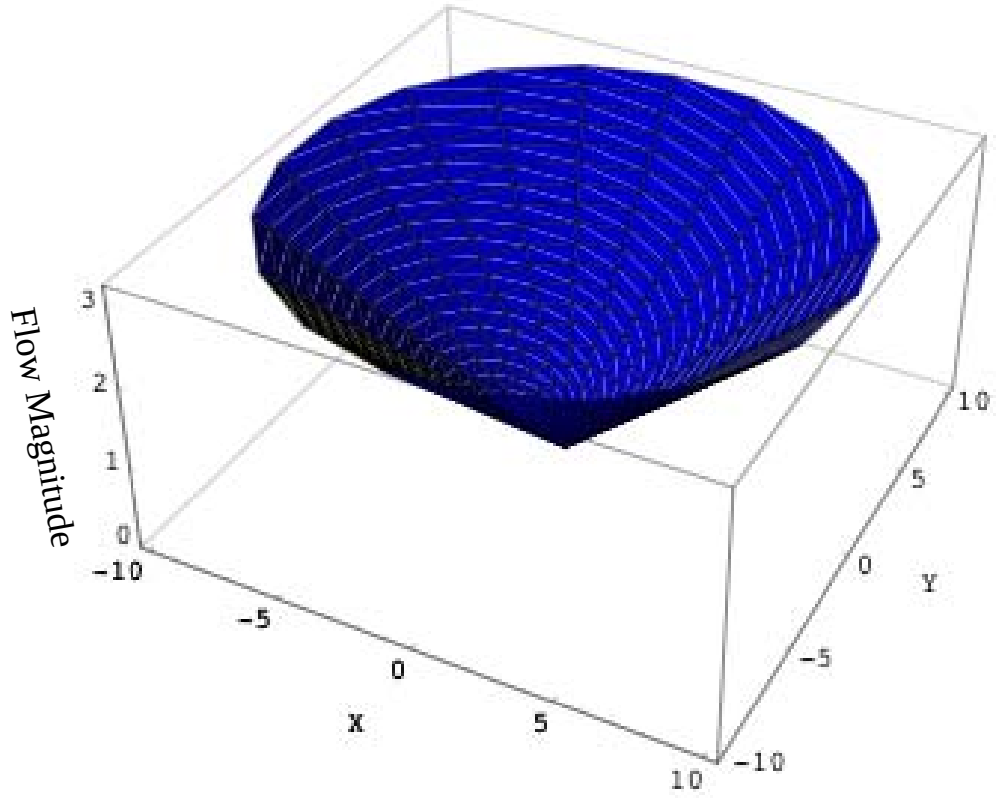

Figure 3-12. Flows, f_{ij}, in the flow field with a circular velocity profile increasing from the center to the outer boundary where the maximum velocity, V_0, equals 3 cm s^{-1}.

Table 12. Flows for circular flow of with maximum velocity V_0 = 3 cm s^{-1} at N = 10. Flows are calculated along the line joining grid points *i* and *i* + 1 and vary only along the radius represented by index *i*. Values have units of cm^3 s^{-1}.

i/i+1 *j*	0	1	2	3	4	5	6	7	8	9	10
0/1	0.15	0.15	0.15	0.15	0.15	0.15	0.15	0.15	0.15	0.15	0.15
1/2	0.45	0.45	0.45	0.45	0.45	0.45	0.45	0.45	0.45	0.45	0.45
2/3	0.75	0.75	0.75	0.75	0.75	0.75	0.75	0.75	0.75	0.75	0.75
3/4	1.05	1.05	1.05	1.05	1.05	1.05	1.05	1.05	1.05	1.05	1.05
4/5	1.35	1.35	1.35	1.35	1.35	1.35	1.35	1.35	1.35	1.35	1.35
5/6	1.65	1.65	1.65	1.65	1.65	1.65	1.65	1.65	1.65	1.65	1.65
6/7	1.95	1.95	1.95	1.95	1.95	1.95	1.95	1.95	1.95	1.95	1.95
7/8	2.25	2.25	2.25	2.25	2.25	2.25	2.25	2.25	2.25	2.25	2.25
8/9	2.55	2.55	2.55	2.55	2.55	2.55	2.55	2.55	2.55	2.55	2.55
9/10	2.85	2.85	2.85	2.85	2.85	2.85	2.85	2.85	2.85	2.85	2.85

The total system throughput, f.., is 165 m^3 s^{-1}. This is easily verified by summing all nonzero flows (Table 12). Organization or the ordered component of the flow is measured by the AMI, which is equal to 6.508 bits of information. The overall network ascendency, A, calculated as A = (AMI) x (f..), is 1,074 flow bits. Identifying which flows make the greatest contribution to the A can be seen by plotting the distribution of the A (Figure 3-13) over the flow field. As one might derive from examining the flow matrix, the flows with the greatest contribution to the A are located along the boundary of the flow field where the velocity is greatest.

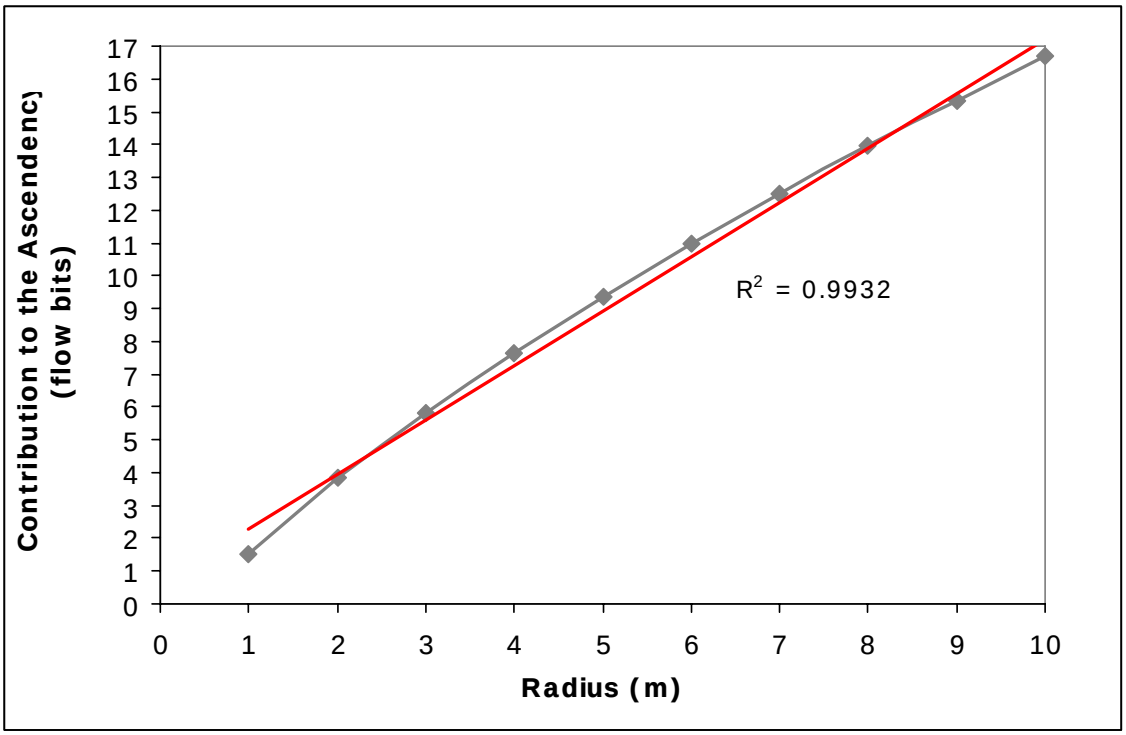

Figure 3-13. Contribution of each flow, f_{ij}, along a single radius in the circular flow field to the overall flow field ascendency. Flow occurs only in the θ-direction and flow velocity, V_θ, is such that $V_\theta = 0$ at r = 0, and V_θ is maximum at r = R = 10 m. Contributions to the ascendency correspond with the velocity and flow profiles.

A similar plot of the distribution of the sensitivities of the A to individual flows along a single radius highlights those flows that exhibit the greatest resistance, or alternatively the least amount of structured activity, to the overall flow within the flow field (Figure 3-14). Areas with the highest sensitivity values are effectively acting as bottlenecks in a flow field. The flows are all structured similarly (i.e. they all map concentric circles within the flow field), so it is the activity (i.e. the sum of the magnitudes of the flows) that differentiates the flows and dominates the sensitivities.

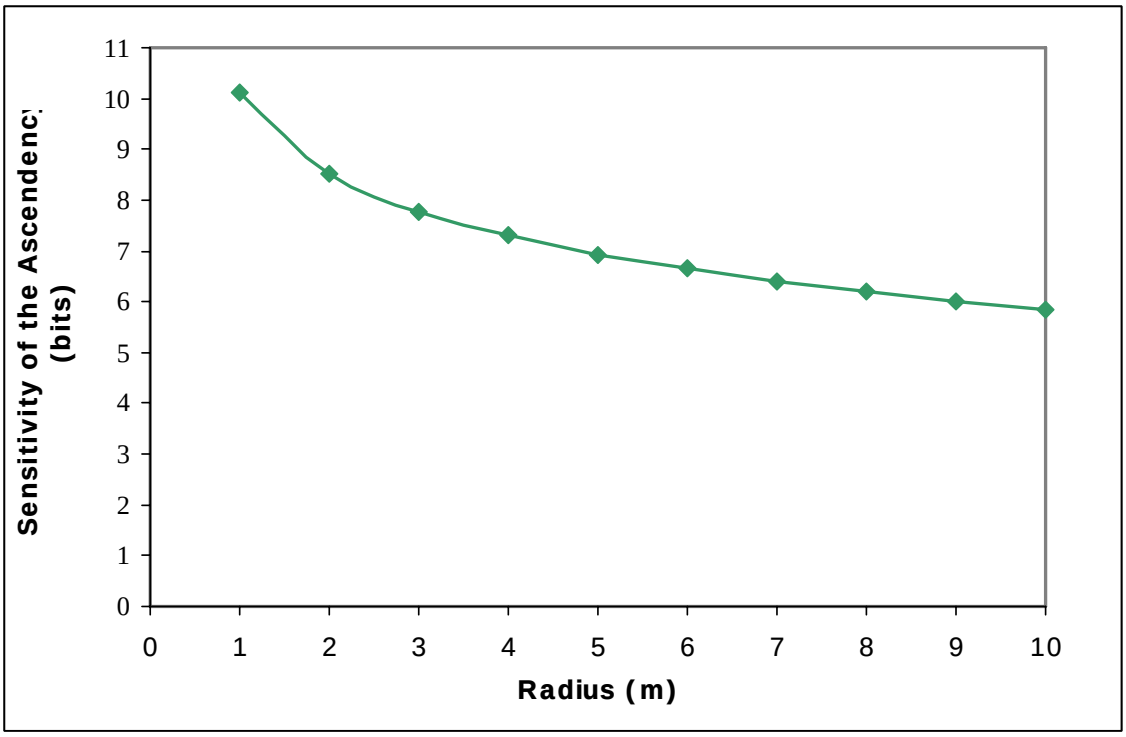

Figure 3-14. Sensitivity of the ascendency to individual flows within the circular flow field along a single radius. Flow is in the θ-direction and flow velocity, V_θ, is such that $V_\theta = 0$ at r = 0, and $V_\theta = V_0 = 3$ cm s^{-1} at r = 10.

Even though the velocity profile increases linearly as a function of R, both the A profile and the sensitivity of the A profile vary as a function of $\log_2$ in the radial direction. This dependency is more pronounced in the sensitivities (Figure 3-14), which are not scaled by the individual flows, and explains why areas of low activity are highlighted in the calculation of the sensitivity of the A to each flow.

3.2 Comparing the network analysis results of the four analytical examples

All four examples were designed to enable a straightforward comparison of the network analysis results generated by each flow field. Values of constants such as the

maximum velocity and variables such as the size of the grid applied to each flow field were purposefully chosen to remain the same in all four examples. These constraints are certainly not essential for a comparison of network analysis results (Ulanowicz 1986a; Ulanowicz and Baird 1999), but they do serve to focus the comparison on the distinctions between the networks, and how those distinctions are represented by the network indices.

The total system throughput for each of the four analytical examples is a function of the velocity profile across each flow field. Summing all flows in a flow field is a holistic way of measuring the flow field activity, a characteristic represented by the f.., and in the case of the four analytical examples, indicates that the parabolic flow profile moves the largest volume of fluid per unit time (Table 13). The f.. provides no indication of flow direction, and it is entirely conceivable to have a flow field with very high activity (f..) and no discernable overall flow; a highly turbulent flow field might be described in such a way.

Table 13. Network indices characterizing the four analytical flow fields.

Flow Field	f.. ($cm^3\ s^{-1}$)	AMI (bits)	A (flow bits)	Maximum Sensitivity (bits)
1. Linear Profile	165	6.508	1,074	10.103
2. Parabolic Profile	220	6.620	1,456	8.617
3. Adjacent Fluids	210	6.618	1,330	8.682
4. Circular Flow	165	6.508	1,074	10.103

The AMI reports the amount of direction in the flow field, or alternatively, is a measure of how well organized the flows are in generating that activity. Flow with a parabolic velocity profile exhibited the highest level of organization (Table 13) with an AMI only slightly greater than the flow of two adjacent immiscible fluids. The higher viscosity of $Fluid_2$ in the third example reduced the velocity in half of the flow field resulting in an asymmetric profile and ultimately in a less organized transfer of fluid, as in comparison to the second example (Table 13). Recalling that the AMI is also referred to as the average mutual constraint (AMC), one may regard the velocity profile of the two adjacent fluids as being less constrained than the parabolic velocity profile.

The example of circular flow differs only qualitatively from the linear velocity profile example (Table 12). This is the case because the wrap around boundary conditions used in the linear profile example result in the same continuous flow normally characteristic only of circular flow. Having equivalent velocity profiles results in identical network indices; and the two flow fields transfer medium with the same level of organization. The highest sensitivity values are found in the two examples with linear flow profiles (Table 12). Even though all four flow fields have at least one boundary where the velocity is zero (also the areas where the sensitivity is highest), the velocity of the non-linear flow profile examples increases more rapidly from $i = 0$ to $i = 1$, so the flows are greater and the sensitivities are less.

As a point of reference, a fifth flow field example consisting of a single fluid flowing between two frictionless boundaries with a uniformly linear velocity profile

where V_x = 1.5 cm s^{-1} between y = 0 and y = R is analyzed as a network. A velocity of 1.5 cm s^{-1} is chosen because it is (or is quite close to) the average velocity for the velocity profiles discussed above. For the uniform flow example, the f.. = 182 cm^3 s^{-1} and the AMI = 6.781 bits resulting in an A of 1,234 flow bits. Uniform flow represents the most highly constrained flow field, and thus an upper limit to the development of any flow field with the same basic characteristics (i.e. laminar flow between two parallel boundaries and wrap around conditions). The uniform flow example is analogous to the maximally organized, minimally connected example from Chapter 1 (Figure 1-1).

Chapter 4. Conclusion

Basic generalized examples of fluid flow are modeled and represented as networks to demonstrate the applicability and potential benefits of network analysis to the characterization of complex systems of fluid flow, such as data from large eddy simulations.

4.1 Summary of results

The technique of cellular automata was used to create three simple flow fields that demonstrate a correlation between the ascendency index, A, and an increase in ordered or directional flow. The correlation is maintained following the introduction of obstructions to the flow field designed to disturb and redirect the otherwise uniform flow. In these cases, the ascendency index is used to highlight areas within the flow field exhibiting the greatest amount of ordered activity. The flows making the greatest contribution to the system ascendency are the flows or pathways of greatest activity. Calculating the sensitivity of the ascendency to individual flows highlights areas in a flow field that exhibit the least amount of ordered activity or the greatest resistance to flow. Examining the contributions to the ascendency and the sensitivities of the ascendency for a given flow field reveals those flows that contribute the greatest to the organization of the flow and those flows that exhibit the greatest resistance to flow, respectively. The highest sensitivity areas correspond with control points or bottlenecks in the flow fields.

In the second approach demonstrating the applicability of network analysis to fluid flow, four analytical examples, familiar to both oceanographers and fluid dynamicists, were modeled and their flows were analyzed as networks. The examples are distinguished by their velocity profiles which are: 1) linear, 2) parabolic, 3) parabolic with two adjacent immiscible fluids, and 4) linear with circular flow. Parabolic flow between two parallel boundaries resulted in the highest ascendency, and is characterized as the most organized flow field. Dividing the flow field in half and assigning a slightly more viscous fluid to one half reduces the velocity in that half of the flow field. A corresponding drop in the total system throughput (f..) and the average mutual information (AMI) was observed. Since the ascendency is a product of these two quantities, a more pronounced reduction in the ascendency was also recoded. In each of the four analytical examples, the highest sensitivity values corresponded well with the regions of the flow field one would intuitively associate with the areas of greatest shear stress. These same areas can be described as exhibiting the greatest resistance to flow and should correspond equally well with bottlenecks to the flow in more complex flow fields.

4.2 Further Research

The flow fields analyzed as networks in this research are simple expressions of fluid flow. To fully demonstrate the usefulness of network analysis to the characterization of fluid flow, actual flows derived from models that take into account the forces driving fluid motion must be analyzed. To characterize turbulent flow and to contribute to the analysis of large eddy simulation data, network analysis must

accommodate flows occurring in three dimensions. This not a strain on the technique; individual cells from a three-dimensional grid can be numbered consecutively from 0 to N and stored in a matrix just as easily as numbering cells in a two-dimensional grid. The difficulty may come in interpreting the network analysis results of these more complex flow fields. An understanding of how network analysis characterizes fluid flows is gained by first investigating simple examples like the ones described in this thesis, and then building on that understanding to the point where more complex and less intuitively obvious flows can be confidently described in terms of their network indices.

Literature Cited

Allesina, S. 2004. Personal communication in person between Mr. Mike Zickel, CBL, and Dr. Stefano Allesina, NOAA. Unpublished code written in the C programming language developed for calculating network indices. Solomons, Maryland. April.

Baird, D. and R.E. Ulanowicz. 1989. The seasonal dynamics of the Chesapeake Bay ecosystem. Ecological monographs 59(4):329-364.

Batchelor, G.K. 1970. An introduction to fluid dynamics. Cambridge, United Kingdom. Cambridge University Press.

Bird, R.B., W.E. Stewart, and E.N. Lightfoot. 1960. Transport phenomena. New York. John Wiley & Sons, Inc.

Boynton, W. 2003. Personal communication in person between Mr. Mike Zickel, CBL and Dr. Walter Boynton, CBL. Ecology seminar. Solomons, Maryland. March.

Chopard, B. and M. Droz. 1998. Cellular automata modeling of physical systems. Cambridge, United Kingdom. Cambridge University Press.

Dewar, R.C. 2005. Maximum entropy production and non-equilibrium statistical mechanics. Pages 41-55 in A. Kleidon and R.D. Lorenz, eds. Non-equilibrium thermodynamics and the production of entropy: Life, earth, and beyond. New York. Springer.

Elert, Glen. 2002. Density of seawater: The physics factbook. Accessed 20 July 2005. http://hypertextbook.com/facts/2002/EdwardLaValley.shtml.

Hagen, J.B. 1992. An Entangled Bank: The Origins of ecosystem ecology. New Brunswick, New Jersey. Rutgers University Press.

Hirata, H. and R.E. Ulanowicz. 1984. Information theoretical analysis of ecological networks. Int. J. Systems Sci. 15:261-270.

Joyce, James. 2003. Bayes' Theorem: The Stanford encyclopedia of philosophy, winter 2003 edition, Edward N. Zalta, ed. Accessed 23 July 2005. http://plato.stanford.edu/archives/win2003/entries/bayes-theorem/.

Kleidon, A. and R.D. Lorenz. 2005. Entropy production by earth system processes. Pages 1-20 in A. Kleidon and R.D. Lorenz, eds. Non-equilibrium thermodynamics and the production of entropy: Life, earth, and beyond. New York. Springer.

Li, M. 2001. Personal communication in person between Mr. Mike Zickel (CBL) and Dr. Ming Li (HPL). Committee Meeting. Cambridge, Maryland.

Lindeman, R.L. 1942. The trophic-dynamic aspect of ecology. Ecology 23:399-418.

Mann, K.H. and J.R.N. Lazier. 1996. Dynamics of marine ecosystems: Biological-physical interactions in the oceans, 2nd ed. Malden, Massachusetts. Blackwell Sciences, Inc.

Mason, P.J. 1994. Large-eddy simulation: A critical review of the technique. Quart. J. Roy. Meteor. Soc. 12:1-26.

Odum, H.T. 1957. Trophic structure and productivity of Silver Springs, Florida. Ecological Monographs 27:55-112.

Odum, E.P. 1969. The strategy of ecosystem development. Science 164:262-270.

Pozrikidis, C. 1999. Little Book of Streamlines. Academic Press. San Diego, CA. p. 148.

R Development Core Team. 2003. R: A language and environment for statistical computing. R Foundation for Statistical Computing, Vienna, Austria. ISBN 3-900051-00-3, URL http://www.R-project.org.

Rutledge, R.W., B.L Basorre, and R.J. Mulholland. 1976. Ecological stability: An information theory viewpoint. J. Theor. Biol. 57:355-371.

Salmon, R. 1999a. The lattice Boltzmann method as a basis for ocean circulation modeling. J. of Marine Res. 57:503-535.

Salmon, R. 1999b. Lattice Boltzmann solutions of the three-dimensional planetary geostrophic equations. J. of Marine Res. 57:847-884.

Tribus M. and E.C. McIrvine. 1971. Energy and information. Scientific American. 225(3):179-188.

Ulanowicz, R.E. 1986a. Growth and development: ecosystems phenomenology. Lincoln, Nebraska. toExcel Press.

Ulanowicz, R.E. 1986b. A phenomenological perspective of ecological development. Pages 73-81 in T.M Poston and R. Purdy, eds. Philadelphia. American Society for Testing and Materials.

Ulanowicz R.E. 1997. Ecology the ascendent perspective. New York. Columbia University Press.

Ulanowicz, R.E. 2000. Quantifying constraints upon trophic and migratory transfers in landscapes. Pages 113-142 in Sanderson, J. and L.D. Harris, eds. Landscape ecology: A top-down approach. Boca Raton, Florida. Lewis Publishing.

Ulanowicz, R.E. and D. Baird. 1999. Nutrient controls on ecosystem dynamics: The Chesapeake mesohaline community. J. Mar. Sci. 19:159-172.

Ulanowicz R.E. and K.H. Mann. 1981. Ecosystems under stress. Pages113-117 in T. Platt, K.H. Mann, and R.E. Ulanowicz, eds. Mathematical models in biological oceanography. Paris. UNESCO.

Ulanowicz, R.E. and M.J. Zickel. 2005. Using ecology to quantify organization in fluid flows. Pages 57-66 in A. Kleidon and R.D. Lorenz, eds. Non-equilibrium thermodynamics and the production of entropy: Life, earth, and beyond. New York. Springer.

Zorach, A.C. and R.E. Ulanowicz. 2003. Quantifying the complexity of flow networks: How many roles are there? Complexity 8(3):68-76.